Pergamon

Geochimica et Cosmochimica Acta, Vol. 68, No. 3, pp. 455–475, 2004

0016-7037/04 $30.00 + .00

doi:10.1016/S0016-7037(03)00457-5

An exotic kind of cosmic material: Graphite-containing xenoliths from the Krymka (LL3.1) chondrite

VIRA P. SEMENENKO,[1,*] AELITA L. GIRICH,[1] and LARRY R. NITTLER[2]

[1]Institute of Environmental Geochemistry, NAS of Ukraine, Palladina 34a, Kyiv-142, 03680, Ukraine
[2]Department of Terrestrial Magnetism, Carnegie Institution of Washington, 5241 Broad Branch Rd., NW, Washington, DC 20015, USA

(*Received September* 5, 2002; *accepted in revised form June* 23, 2003)

Abstract—Seven graphite-containing xenoliths were found in the Krymka (LL3.1) chondrite. The xenoliths have the following chemical and mineralogical characteristics which distinguish them from the Krymka host: (1) low totals in bulk chemical analyses obtained by electron microprobe; (2) high bulk Fe abundances; (3) a uniform recrystallized, chondrule-free texture; (4) the presence of euhedral graphite and carbon-rich material; (5) higher quantities of troilite and metal; (6) a relatively homogeneous composition of silicates; (7) a distinctive composition of metal, chromite and phosphate; (8) isotopically heavy C in graphite compared to both bulk Krymka and graphite in other ordinary chondrites. The xenoliths are mineralogically similar, but not identical, to the Krymka carbonaceous clast K1, which bears graphite microcrystals, organic compounds and mysterite. They resemble carbonaceous chondrites, both chemically and isotopically. The mineralogical, chemical and isotopic data for the graphite-containing fragments suggest that this material represents metamorphosed varieties of a previously unknown type of unequilibrated carbonaceous matter. Most likely, the graphite has a metamorphic origin and was crystallized from C-containing precursor materials through the following transformation sequence: organic compounds → C-rich material → graphite.

1. INTRODUCTION

The known types of meteorites represent a narrow spectrum of the materials formed in the solar system. In this connection, searches for and studies of new kinds of cosmic material are of high scientific interest. Many meteorites, especially the unequilibrated ordinary LL-chondrites, bear abundant xenoliths (Kurat, 1970; Fodor and Keil, 1978; Huss, 1979; Wlotzka, 1983; Endress et al., 1994), some of which belong to exotic samples and can provide fundamental information about early processes in the solar nebula.

The Krymka chondrite (LL3.1) contains various kinds of xenoliths, consisting mainly of mafic minerals (Semenenko et al., 1991a,b, 1998, 2001; Semenenko and Girich, 1995; Semenenko, 1996). The xenoliths are classified into three mineralogical groups on the basis of their mineralogy: sulfide-enriched, metal-enriched and silicate (Semenenko and Girich, 2001). Sulfide-enriched xenoliths are predominant in Krymka. Some of these, especially graphite-containing xenoliths, represent an exotic kind of cosmic material (Semenenko and Girich, 1995, 1996, 1998). Graphite is a rare mineral in some iron meteorites (Mason, 1963), ureilites, enstatite chondrites (Ramdohr, 1973), carbonaceous and unequilibrated ordinary chondrites (Mostefaoui et al., 1997). In the latter cases, some graphite microcrystals have a presolar origin (Amari et al., 1990; Zinner et al., 1990, 1995). In contrast to all known meteoritic graphite types, those of the xenoliths discussed here are abundant and form large euhedral crystals.

Mineralogical studies of the first graphite-containing xenolith to be identified, which is a fragment of a larger primary body, suggested that it originated as a result of crystallization from a highly reduced silicate melt enriched in carbon (Semenenko and Girich, 1995). The fragment is basically characterized by a granular texture without chondrules, the presence of uniformly distributed graphite crystals, slightly inhomogeneous compositions of silicates, and mineral compositions distinctive from those of the Krymka host.

Here we present the results of a petrographic, mineralogical and isotopic study of seven graphite-containing fragments. The present results revise our previous understanding of the nature of the graphite-bearing material. They testify that the graphite-bearing material of the fragments most likely represents metamorphosed varieties of a previously unknown type of unequilibrated carbonaceous matter.

2. SAMPLES AND ANALYTICAL PROCEDURES

Seven graphite-containing fragments (Gr1–Gr7) were found on broken surfaces of the individual sample N 1290/29 (catalogue number of the meteorite collection of the Museum of Natural History, NAS of Ukraine). This sample has been shocked more intensively than the rest of the meteorite and contains regions of completely shock-melted material (Semenenko and Perron, 1995, 1996).

Splinters from the fragment Gr1 ($<0.3 \times 0.5$ mm in size) were examined by scanning electron microscopy (SEM) to study morphologic features of the broken surface, and by transmitted light microscopy to investigate evidence for shock metamorphism in olivine. Polished sections of all seven fragments were prepared for petrographic study by reflected light microscopy and SEM (REM-100u, JCXA-733 and Jeol JSM-840A, Kyiv and Paris) using energy dispersive spectroscopy (EDS), as well as field-emission SEM (Jeol JSM-6300F, Münster). Mineral compositions were determined by electron microprobe (EMP) (JCXA-733 Jeol Superprobe, Kyiv; Cam-

* Author to whom correspondence should be addressed (virasem@i.com.ua).

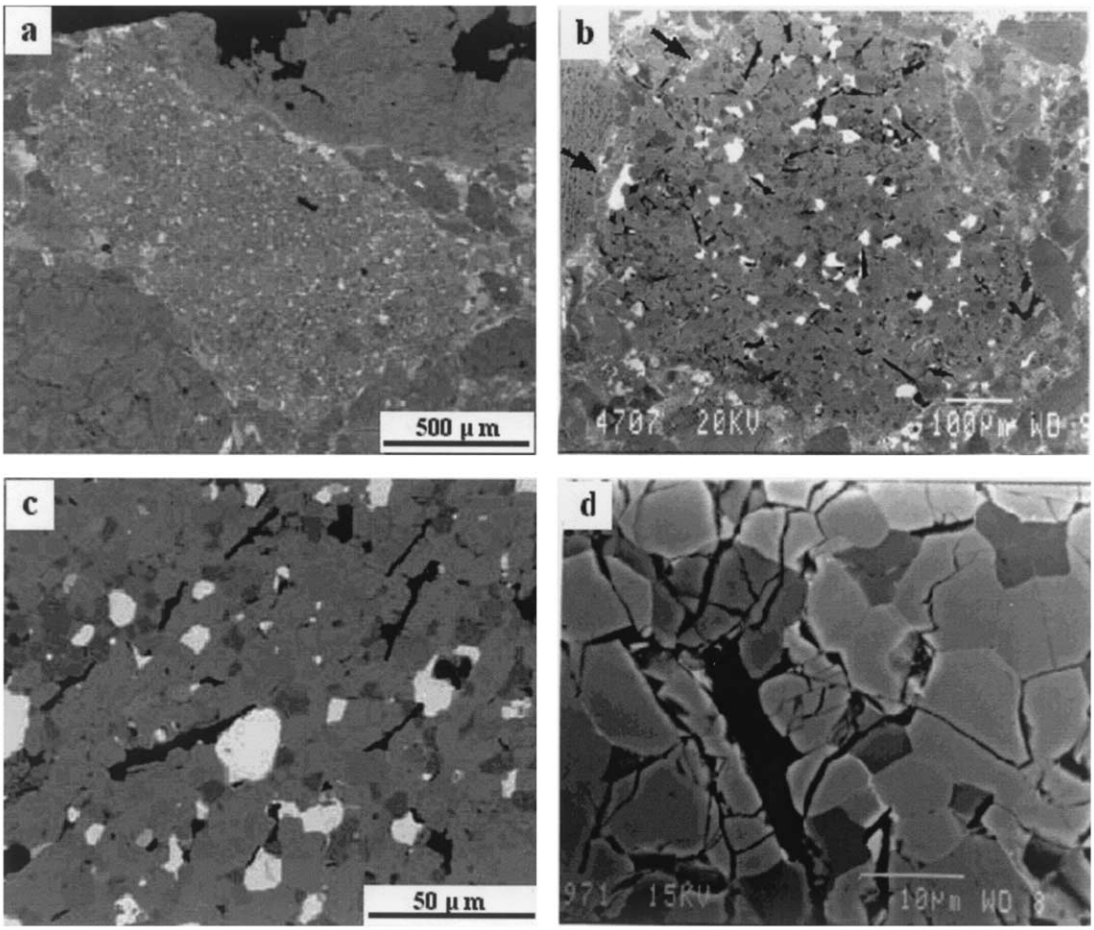

Fig. 1. Backscattered electron (BSE) images of the graphite-containing fragments in the Krymka polished sections. The fragments are uniformly recrystallized and chondrule-free. (a) The fragment Gr7. Troilite (white) is uniformly dispersed among silicates (grey, dark-grey) of the fragment. Two of the largest black spots on the right-hand side of the fragment are contamination. (b) The fragment Gr6. Graphite is black, troilite and metal are white, silicates are light-grey and grey. Note a fine-grained discontinuous rim (arrows) on the left-hand side of fragment. (c) Uniformly granular texture of the fragment Gr2. Some graphite crystals are bent and restricted to interphase boundaries. Graphite is black, troilite and metal are white, silicate is grey. (d) Details of the granular texture showing clear evidences of recrystallization—prominent triple junctures and straight or slightly curved interfacial boundaries, within the fragment Gr6. This area of the fragment is intensively brecciated. Olivine is light-grey, pyroxenes are grey, plagioclase is dark-grey and graphite crystals are black.

ebax-36 and Cameca SX-50, Paris; and JXA-8900R, Washington, DC). The electron microprobes operated at accelerating voltages of 10 kV for graphite crystals, 15 kV for silicates and 25 kV for metallic phases. The beam currents were 50 nA for graphite and 10 nA for the other minerals, with a 2-μm average diameter. Well-known minerals served as standards and all analyses were corrected using a ZAF routine. The bulk compositions of the fragments were obtained using a defocused beam (20 μm).

Carbon and nitrogen isotopic compositions were determined for three graphite crystals with a Cameca ims-6f ion microprobe (Carnegie Institution of Washington). A 17.5-keV Cs^+ primary ion beam was focused to a spot a few micrometers across. Secondary ions of ^{12}C, ^{13}C, $^{12}C^{14}N$ and $^{12}C^{15}N$ were detected in peak-jumping mode. A mass resolving power of 5000 was sufficient to resolve important isobaric interferences. An electron flood gun was used to compensate for possible sample charging. Conducting graphite paint was used as an isotopic standard.

The studies were performed in the Institute of Environmental Geochemistry NAS of Ukraine (Kyiv), Smithsonian Institution (Washington, DC), Museum Nationalle de Histoire Naturelle (Paris), Carnegie Institution of Washington (Washington, DC), and partially in the Institute of Planetologie (Münster).

3. RESULTS

3.1. Petrography and Mineralogy

The graphite-containing fragments Gr1 to Gr7 are dark, friable and chondrule-free. Examination of polished sections showed the xenoliths have a sharp boundary with the Krymka host (Figs. 1a and 1b) and are surrounded by relics of a fine-grained silicate rim (Fig. 1b). Their main macroscopic and mineralogical features are given in Table 1.

Table 1. Mineralogical and some chemical characteristics of the graphite-containing xenoliths in the Krymka thick polished sections.

				Mineralogical composition						
Xenoliths	Apparent size (mm)	Shape	Fine-grained rim	Olivine, pyroxenes, feldspatic plagioclase	Graphite (crystals)	Metal, sulfides	Chromites	Phosphates	Other opaques	FeO / (FeO + MgO)
Gr1	2.4 × 2.6	5-angular	Continuous	$Fa_{31.2}$; $Fs_{23.2}$; $Fs_{10.7}Wo_{43.2}$; $Ab_{82.4}Or_{0.4}$	Coarse, fine	Awaruite, troilite, pentlandite	Chromite (2 groups)	F-apatite, merrilite	Magnetite	0.51
Gr2	0.7 × 0.8	4-angular	Continuous	$Fa_{29.6}$;$Fs_{23.4}$;$Fs_{11.5}Wo_{42.0}$; $Ab_{81.3}Or_{0.2}$	Coarse, fine	Taenite, kamacite, troilite	Chromite	Cl-apatite, merrilite		0.54
Gr3	0.6 × 0.9	3-angular	Discontinuous	$Fa_{37.1}$;$Fs_{23.4}$;$Fs_{9.5}Wo_{45.4}$; $Ab_{81.1}Or_{0.6}$	Fine	Awaruite, taenite, troilite	Chromite (2 groups), Cr-spinel	F-apatite, merrilite	Magnetite, ilmenite	0.59
Gr4	0.6 × 0.6	8-angular	Discontinuous	$Fa_{32.8}$; $Fs_{23.6}$; $Fs_{10.1}Wo_{43.9}$; $Ab_{82.5}Or_{0.7}$	Fine, coarse	Awaruite, taenite, kamacite, troilite	Chromite	Merrilite		0.55
Gr5	1.3 × 1.7	4-angular		$Fa_{32.0}$; $Fs_{23.5}$; $Fs_{13.2}Wo_{39.3}$; $Ab_{81.2}Or_{0.2}$	Coarse, fine	Awaruite, taenite, troilite	Chromite	F-apatite, merrilite	Magnetite	0.54
Gr6	0.6 × 0.7	Rounded	Discontinuous	$Fa_{25.6}$; $Fs_{21.5}$; $Fs_{9.3}Wo_{44.4}$; $Ab_{81.0}Or_{0.1}$	Coarse, fine	Awaruite, taenite, kamacite, troilite	Chromite	Cl-apatite		
Gr7	0.8 × 1.5	5-angular	Discontinuous	$Fa_{31.5}$; $Fs_{20.4}$; $Fs_{8.7}Wo_{44.8}$; (1) $Ab_{90.8}Or_{3.0}$, (2) $Ab_{15.1}Or_{0.3}$	Fine	Awaruite, taenite, kamacite, troilite	Chromite (2 groups)	Cl-apatite	Wustite	0.53

The fragments exhibit a uniform recrystallized texture (Figs. 1c and 1d), comprised of mineral grains predominantly <50 μm in size. The largest grains are polymineralic with an anhedral shape and consist of olivine and/or pyroxenes and plagioclase. Small silicate grains (≤10 μm) are monomineralic, dominated by a subhedral or euhedral shape. The grain boundaries between many of the individual crystals of silicates are straight or slightly curved indicating that these clusters are at textural equilibrium (Fig. 1d). The fragments contain mainly silicates and troilite, minor graphite, metal, chromite, phosphates and magnetite (Table 1). According to a quantitative estimation, the fragment Gr1 contains the following minerals (vol.%): *silicates* (*olivine, pyroxenes and plagioclase feldspar*) = 78.7; *troilite*= 11.3; *graphite* =3.0; *awaruite* = 2.2; *magnetite*= 2.9; both chromite and phosphates <1 and rare grains of pentlandite; *total* (*excluding holes*) =100%. Like the rest of the fragments, Gr1 contains 14 vol.% of artificial holes caused by plucking of mineral grains during grinding and polishing of samples.

3.1.1. Silicates and phosphates

Olivine is the most widespread phase within the fragments, its composition (Appendix, Table A1) is slightly inhomogeneous within and between the fragments. In most cases, Fa-content (Fig. 2) is higher than that of equilibrated LL-chondrites. Olivine in fragment Gr6 contains the lowest Fa, fragment Gr3 the highest. Olivine composition is similar both in Gr1 and Gr4, and in Gr5 and Gr7. Within Gr3, Gr6 and Gr7 the olivine composition is more homogeneous than within the rest. One olivine grain in Gr1 (composition [wt.%]: 36.2 SiO_2; 32.8 MgO; 27.8 FeO; 3.00 P_2O_5; 0.36 MnO; 0.09 CaO; 0.06 Cr_2O_3; 0.05 TiO_2; total 100.4; $Fa_{32.2}$), resembles phosphoran olivine in pallasites (Semenenko and Girich, 1995).

Pyroxene, primarily Ca-poor and to a lesser extent Ca-rich, is also an important constituent of the graphite-bearing xenoliths. Pyroxene composition (Appendix, Table A1; Fig. 2) is slightly inhomogeneous within and between the fragments (except for Gr7) and corresponds to that of the equilibrated LL- or L-chondrites. Most grains of Ca-poor pyroxene in Gr7 are hypersthene, but some of them are enstatite or bronzite. Fragments Gr3, Gr5 and Gr6 have the most uniform Ca-poor pyroxene compositions, whilst the most homogeneous Ca-rich pyroxenes are within Gr3, Gr6 and Gr7 (Fig. 3).

Feldspathic plagioclase grains have anhedral and in rare cases euhedral shape. Their composition (Appendix, Table A1) is uniform and similar for the different fragments (Fig. 4). Two compositional groups of plagioclase have been found in Gr7: most grains have a typical oligoclase composition ($An_{6.36}$), but some grains are anorthitic ($An_{84.7}$).

Phosphate grains are composed of merrilite and Cl-apatite, which are typical for chondrites. Some of the fragments also contain F-apatite, which is rare in chondrites. The composition of the phosphates (Appendix, Table A2) slightly varies within and among the fragments.

3.1.2. Graphite

Graphite crystals are uniformly distributed within the fragments. In polished sections, most have a regular lamellar shape (Figs. 5a–5e), although some are irregular. Lamellar grains with a length/width ratio much greater than 10 are rare. There was one pyramid-shaped grain, presumably from a pyramidal pseudoform. There are two groups of euhedral graphite crystals, which differ in size and occurrence within the fragments. Coarse graphite grains (<120 × 6 μm) are arranged among silicates and opaque minerals. Many of the coarse graphite crystals are larger than the minerals located on their phase boundary (Fig. 5a). Some of these are bent (Fig. 1c). From bireflection, some crystals display a uniform grey color, indicating a monocrystalline structure, while others exhibit a spotty color (from grey to greyish brown), apparently linked to a polycrystalline structure. The coarse crystals are abundant in the fragments Gr1, Gr5 and Gr6, and absent in the fragments Gr3 and Gr7. The overwhelming majority of fine crystals (<5 × 1 μm) are located on the interphase boundaries of minerals. Some of these partially penetrate into silicate grains (Figs. 5c and 5d), or decorate adjacent faces of minerals and form twins. Rare fine crystals are included in silicate grains. In contrast to the coarse crystals, the fine crystals are present in all of the fragments.

We do not yet have direct data on the morphology of the coarsely-crystalline graphite. An overwhelming predominance of graphite lamellae in the polished sections allows us to suppose that in most cases the graphite forms very thin (a few micrometers) hexagonal plates and we observe their prismatic sections. This supposition is also supported by an SEM investigation of the morphology of graphite microcrystals on a broken surface of Gr1, which showed the presence of regular hexagonal plates (Semenenko and Girich, 1995), with a morphology typical of graphite (Figs. 5e and 5f). Microcrystals of graphite protrude from the surface of silicate grains, metal and troilite globules or are scattered over their surfaces and on the walls of silicate voids.

In a polished section of Gr5, we found a coarse graphite crystal with an intact real face (Fig. 6). One prismatic face of the crystal is located slightly below the surface of the polished section (Fig. 6a), so that its microsculptural features were not destroyed during polishing of the sample. High-magnification secondary electron imaging of this face showed a high porosity of the graphite and a fine-scaly sculpture. Some scales have a nearly regular hexagonal shape (Fig. 6b), suggesting a polycyclic growth of microcrystallites on the surface of the graphite-host. Some surface areas have a globular sculpture. These very limited data allow us to propose a metamorphic growth of graphite microcrystals on the face of the coarse graphite crystal.

Electron microprobe data for the fragments Gr1 and Gr2 show that the graphite consists basically of carbon (95.31–99.91 wt.%) with only small amounts of other elements (wt.%): 0.38 to 1.98 Fe; 0.12 to 0.85 Si; <0.02 to 0.38 Mg; <0.01 to 0.35 Ca; <0.01 to 0.29 Al; n.d. to 0.26 Na; n.d. to 0.26 Ni; <0.01 to 0.14 Cl; <0.00 to 0.11 K and <0.01 to 0.09 S, which may result from a partial contamination of surrounding minerals. Compositional variation is negligible within graphite crystals, but is greater between the crystals.

3.1.3. C-Rich material

C-rich material (perhaps not graphitized) is found mainly in Gr7 (Figs. 7a–7e) as irregular areas inside of feldspar or feldspathic mesostasis, as rare round inclusions inside silicates, and as veins that intrude the interphase boundaries and silicates along fractures. Simultaneous backscatter and secondary elec-

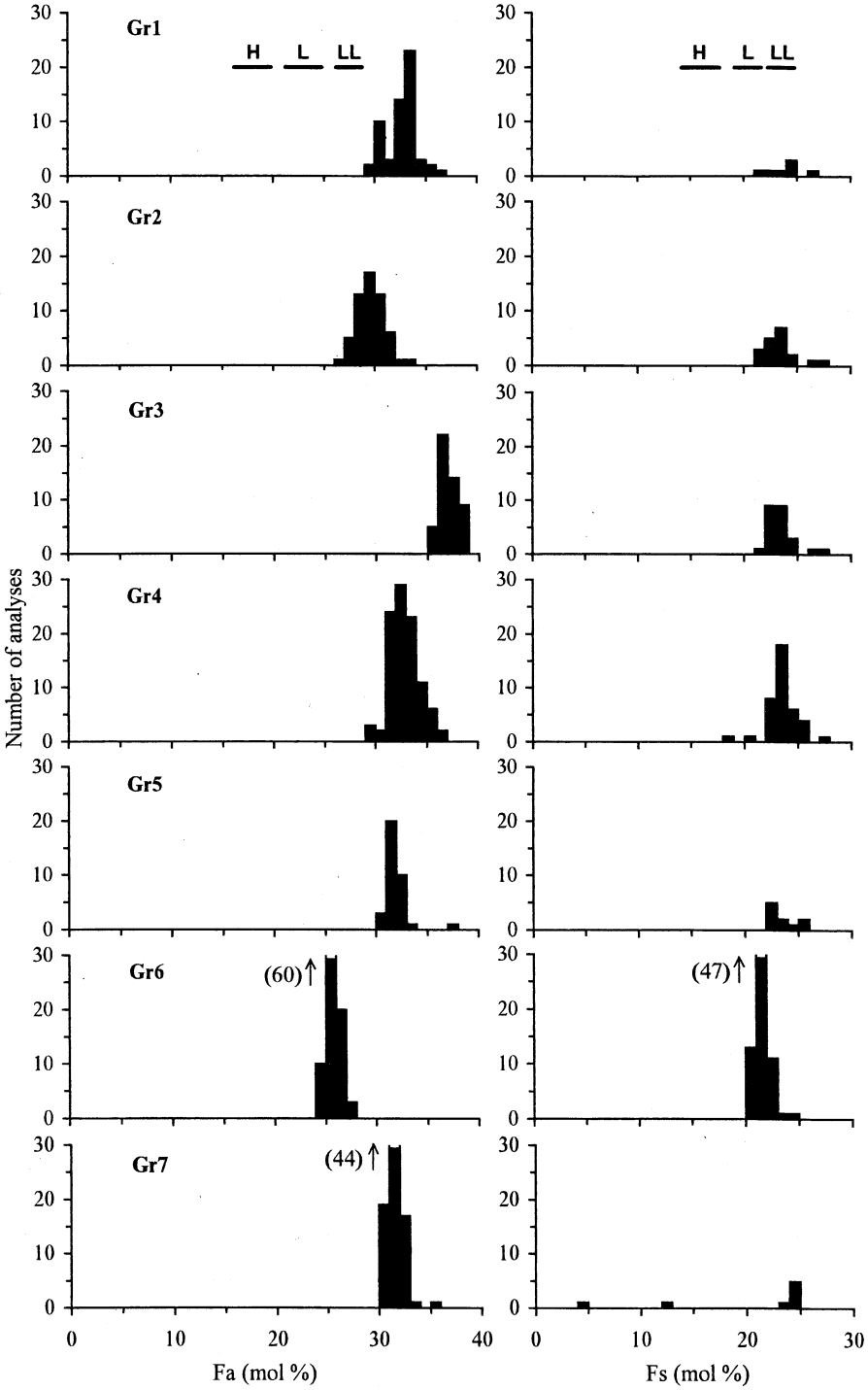

Fig. 2. The Fa-contents of olivine and Fs-contents of Ca-poor pyroxene within the studied fragments Gr1 to Gr7. H, L, LL compositional ranges for olivine and Ca-poor pyroxene from Keil and Fredriksson (1964).

tron imaging indicates that these C-rich areas consist of dark-grey or black material, apparently amorphous, and contain separate pores or rare shrinkage cracks. EDS data confirmed that this material is highly enriched in carbon. In some cases a transition of the C-rich material to regular graphite crystals is clearly visible (Fig. 7f).

3.1.4. Troilite and metal

Troilite is the most widespread opaque mineral. Irregular, sometimes lamellar, hexagonal and cubic troilite grains are uniformly distributed within the fragments. The irregular grains are associated with taenite and the lamellar ones with graphite.

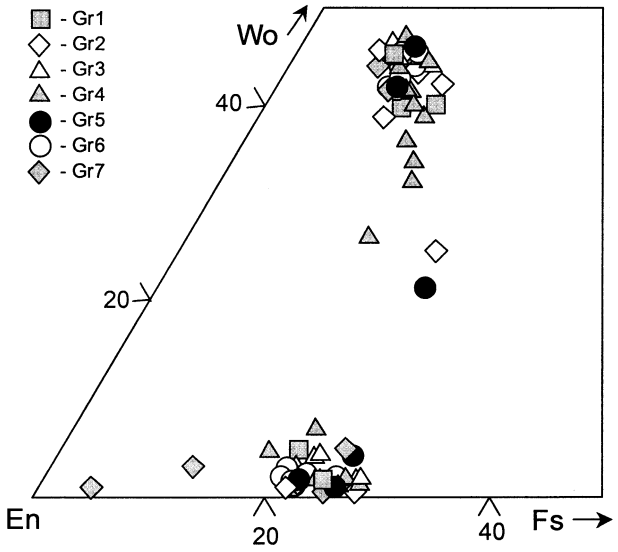

Fig. 3. Chemical composition of Ca-poor and Ca-rich pyroxenes within the graphite-containing fragments.

Cubic crystals of troilite with regular octagonal and tetragonal shapes contain metal relicts. Troilite composition (Appendix, Table A3) slightly varies from grain to grain and small amounts of Ni and Co are present in some points.

Metal consists of Ni-rich taenite (containing up to 67 wt.% Ni, i.e., awaruite), taenite and kamacite. In most cases, the metal is associated with troilite, more rarely with chromite and graphite. The phase composition of metal is different between the different fragments. For example, Gr1 contains only awaruite, while Gr4, Gr6 and Gr7 incorporate awaruite, taenite and kamacite. The chemical composition of the metal (Appendix, Table A3) is variable within and among the fragments. The presence of a high concentration of Co, corresponding to that in kamacite and in some taenite grains from the Krymka matrix, is the main compositional feature of the awaruite. In contrast to taenite from the host chondrite, the Co-content in the awaruite correlates linearly with the concentration of Ni (Fig. 8). The linear correlation is clearly visible within the individual fragments (e.g., see Semenenko and Girich, 1995; Fig. 5) especially in cases where a minimum of ten grains was analyzed. Some uncertainty in Figure 8 is caused by a low quantity of measurable awaruite grains in Gr2 and Gr4. A high content of Co is found also in some taenite grains of Gr5.

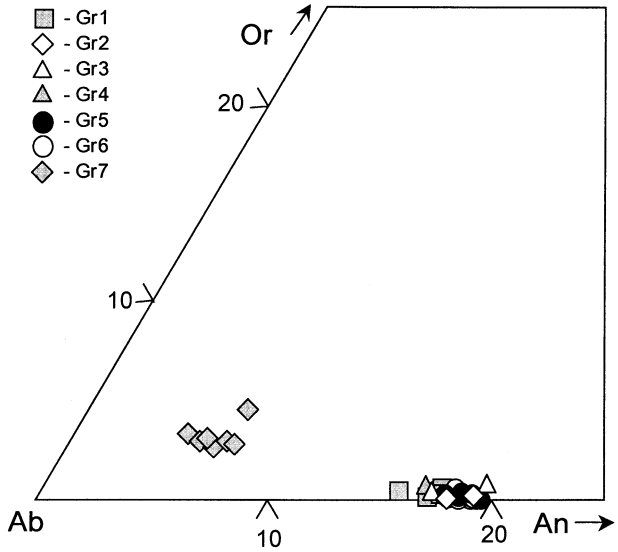

Fig. 4. Chemical composition of feldspatic plagioclase within the fragments Gr1 to Gr7. One grain of the plagioclase ($Ab_{15.09}An_{84.65}Or_{0.26}$) within the fragment Gr7 is disposed outside of the compositional field.

3.1.5. Chromite, magnetite and additional minor minerals

Chromite occurs mainly as rounded grains and in some cases (for example in Gr6) as regular crystals up to 20 μm in size. The composition of chromite (Appendix, Table A4) is variable within and between the fragments and is characterized by high concentrations of TiO_2, MgO and Al_2O_3. The highest concentrations of TiO_2, Al_2O_3 and MgO in chromite are respectively 4.44 wt.% in Gr6, 15.1 wt.% in Gr4, and 6.64 wt.% in Gr7. The largest grain in Gr1 is zoned, with TiO_2, MgO, MnO and V_2O_3 decreasing towards the grain rim.

Two compositional groups of chromite (Appendix, Table A4) can be distinguished within Gr1, Gr3 and Gr7 (although their presence is not excluded from the other fragments, since only a small number of grains were measured, for example 2 or 3 grains within Gr2 and Gr5, respectively). Cr-spinel was also found in Gr3. The composition of Cr-spinel slightly varies from grain to grain (wt.%): 53.0 to 56.0 Al_2O_3; 23.1 to 24.4 FeO; 10.9 to 11.4 MgO; 6.54 to 7.72 Cr_2O_3; 0.17 to 2.46 TiO_2; 0.20 to 0.57 SiO_2; 0.34 to 0.44 V_2O_5; 0.08 to 0.27 P_2O_5; 0.10 to 0.18 MnO; 0.07 to 0.14 CaO and n.d. to 0.14 Na_2O.

Magnetite occurs both as individual grains and in association with troilite and metal within Gr1, Gr3 and Gr5. In some cases, magnetite replaces troilite forming hexagonal crystals like troilite. No cubic magnetite was observed. Composition of magnetite (30.8 wt.% FeO and 68.6 wt.% Fe_2O_3) is similar in different fragments.

Rare grains of *wüstite* (98.1 wt.% FeO), *ilmenite* (49 wt.% TiO_2) and *pentlandite* (50.6 wt.% Fe; 33 wt.% S; 15.1 wt.% Ni; 0.45 wt.% Co; 0.19 wt.% Cu; $<$0.03 wt.% Cr; $<$0.03 wt.% Si; in total 99.4 wt.%) were found in some fragments. Pentlandite is associated with troilite and is arranged on a margin of Gr1. These data testify to a secondary origin of the pentlandite, as a result of terrestrial oxidation of troilite.

3.1.6. Evidence of shock metamorphism

Although the Krymka sample N 1290/29 was shocked more intensively than the rest of the meteorite (Semenenko and Perron, 1995, 1996) the studied fragments contain only limited evidence of deformation and heating. Their silicates are cracked and in some cases are brecciated (Fig. 1d). Taking into account the high friability of graphite-bearing material, formation of the cracks as a result of polishing cannot be excluded. At the same time, it is clear that some cracks were formed

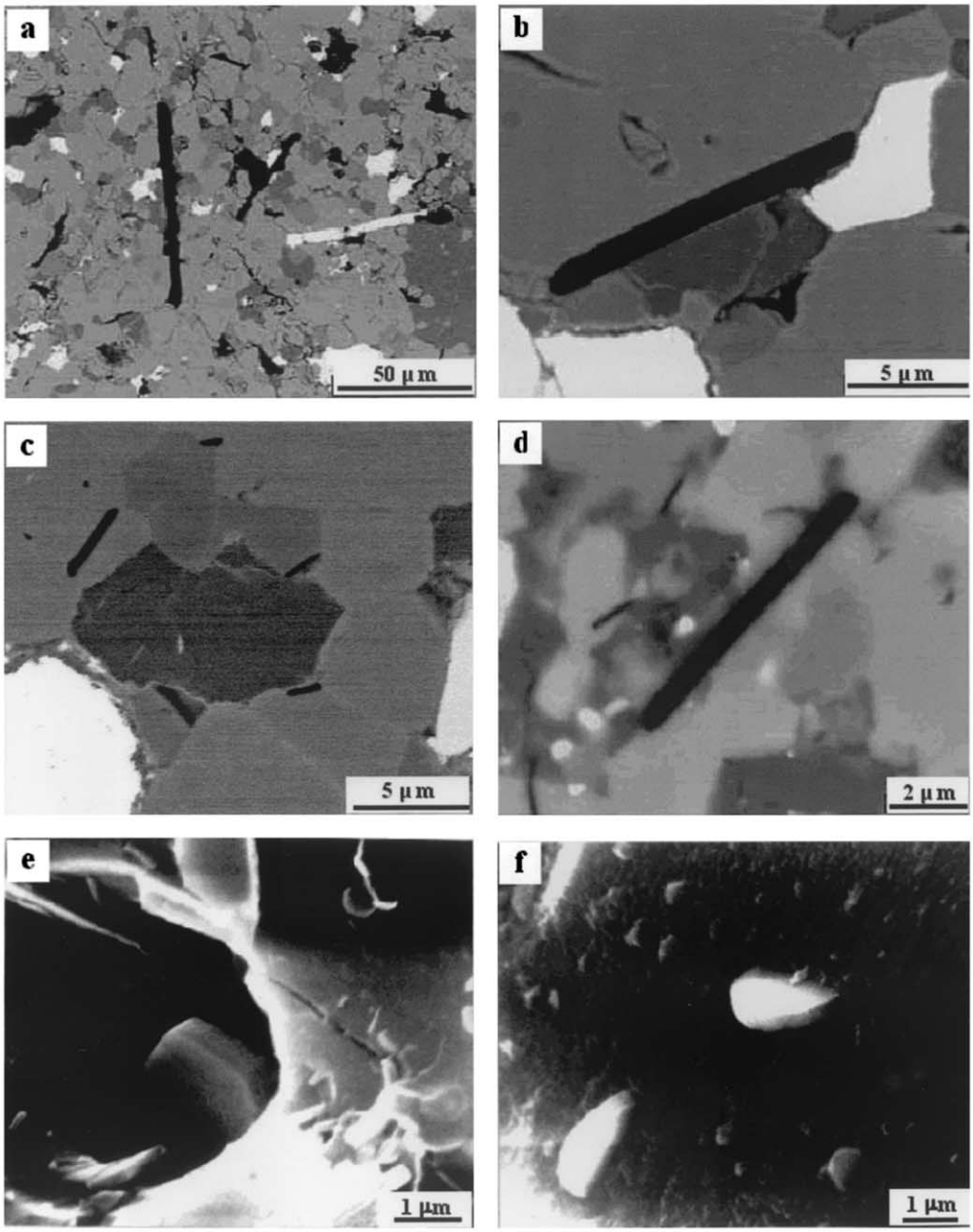

Fig. 5. BSE (a–d; polished sections) and secondary electron (SE) (e, f; a fracture surface) images of graphite crystals arranged within the studied fragments of Krymka. On the BSE images graphite is black, silicates—from light-grey to dark-grey, troilite and metal are white. (a) Coarse graphite lamellars located within the fragment Gr5. Some troilite grains exhibit rare for troilites lamellar shape. (b) One of the coarse graphite crystals arranged on an interphase boundary of minerals within the fragment Gr2. (c) Distribution of fine graphite crystals within the fragment Gr2. (d) Coarse and fine graphite crystals within the fragment Gr7. (e) Graphite microcrystal located inside a void in silicate. The fragment Gr1 (Fig. 2a of Semenenko and Girich, 1995). (f) Protruding microcrystals of graphite on the surface of an olivine grain. The fragment Gr1 (Fig. 2b of Semenenko and Girich, 1995).

during shock metamorphism in space. This conclusion is supported by the following features: the presence of veins of a C-containing material within the cracks of the brecciated silicate areas, undulatory and rare mosaic extinction of olivine grains, and the presence of somewhat curved graphite lamellars. Moreover, the shape of troilite grains in Gr4 is very irregular with some forming melting structures.

3.2. Bulk Chemical Compositions

Bulk chemical compositions of the fragments, as determined by electron microprobe, have low totals (92.0–97.8 wt.%), owing to the presence of graphite and C-bearing material, as well as cracks and abundant artificial holes formed by plucking of mineral grains (mostly troilite) during grinding and polishing

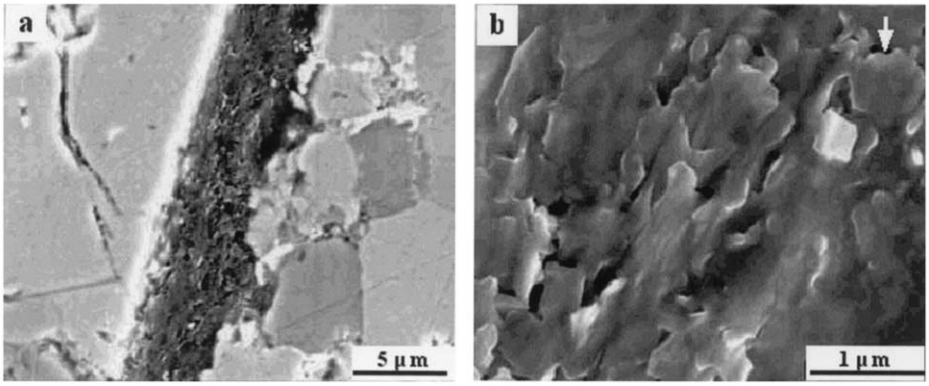

Fig. 6. SE images of a surface of an intact real face of a coarse graphite crystal arranged within the fragment Gr5. The Krymka polished section. (a) A part of the coarse graphite crystal. The surface of the face exhibits a fine-scaly sculpture and high porosity. Such as the crystal face is located a little bit lower than the polished section the surrounding minerals (from light- to dark-grey—silicates; white—troilite and metal) are not in focus. (b) Sculptural details of the graphite face in a high magnification. Some scales (arrow) have a nearly regular hexagonal shape. Separate areas of the surface have an obscure fine globular sculpture.

of the samples. Taking into account the beam size, which is comparable to that of the mineral grains and faults in the polished samples, measured bulk compositions of the fragments have to be considered as approximate. SiO_2/MgO ratio of most fragments varies in range 1.37 to 1.44, similar to that of carbonaceous chondrites (1.42 ± 0.05) (van Schmus and Wood, 1967).

The microprobe data indicate that the graphite-bearing fragments have closely similar bulk compositions, which basically differ in their FeO-contents. The FeO/(FeO + MgO) ratio varies from 0.51 to 0.59 (Table 1) and is higher than that of the Krymka host (0.50). The highest FeO-content is in Gr3 (31.8 wt.%) and the lowest one in Gr1 (26.9 wt.%).

3.3. Isotopic Measurements

Three coarse graphite crystals from fragment Gr6 were analyzed for C and N isotopic compositions. The $\delta^{13}C_{PDB}$ values for the three grains are identical within errors (2.0 ± 5.0, 2.4 ± 4.4, and –1.2 ± 4.8‰, 1σ errors) (Fig. 9). N isotopic compositions are all within errors of terrestrial (average $\delta^{15}N = 10 \pm 18$‰). N contents are low, with CN^-/C^- ion ratios $\sim 10^{-3}$, corresponding to ~70 ppm N in the graphite.

4. DISCUSSION

The mineralogy of the fragments, especially the presence of euhedral graphite crystals and C-rich material, indicate that the fragments represent a foreign material, which is fundamentally different from the Krymka host and distinctive from any other known kind of C-bearing meteoritic material. This means that the primary composition and preaccretion history of these xenoliths and the Krymka main constituents were different. The fragmentary shape (Table 1; Figs. 1a and 1b) directly indicates that these samples were formed as a result of impact fragmentation of a larger lithic rock (or rocks) before or during accretion with typical chondritic material. This conclusion is consistent with data about preferential impact fragmentation of the Krymka large components, e.g., precursors of lithic fragments (Semenenko et al., 2001) and large chondrules (Nelson and Rubin, 2002). This attests to an important role of a shock in the preaccretional history of the Krymka parent body.

4.1. Relationship of the Xenoliths to the Krymka Host

The graphite-containing fragments have the following chemical, mineralogical, and isotopic characteristics, which distinguish them from the Krymka host: (1) low totals in bulk chemical analyses mostly due to presence of graphite and C-rich material; (2) higher bulk Fe abundances; (3) resemblance of their SiO_2/MgO ratio to that of carbonaceous chondrites; (4) a uniform recrystallized, chondrule-free texture; (5) the presence of graphite and C-rich material; (6) higher quantities of troilite and metal; (7) a relatively homogeneous composition of silicates in contrast to that of chromites and metal; (8) a distinctive composition of metal, chromite and phosphate; and (9) isotopically heavy C in graphite compared to both bulk Krymka and graphite in other ordinary chondrites.

4.1.1. Textural features

In contrast to the Krymka host, the fragments do not contain chondrules or their relics. The xenoliths have clear recrystallized textures with prominent triple junctions and slightly curved silicate interfacial boundaries. Many of the mineralogical features attest to recrystallization, which is typical for equilibrated chondrites. For example, the dominant minerals olivine and Ca-poor pyroxene are characterized by uniform grain size and a remarkably narrow range in composition ($Fa_{24.5–38.9}$; $Fs_{20.6–27.5}$, respectively) compared with those of the Krymka host ($Fa_{0–94}$; $Fs_{0–32}$, respectively). Compositional variations in olivine and Ca-poor pyroxene in the fragments (Fig. 2) are closer to (but not identical with) those of equilibrated (Keil and Fredriksson, 1964) rather than unequilibrated chondrites. The fragments also exhibit a higher quantity and coarser grain sizes of metamorphic minerals such as feldspathic plagioclase, chromite and phosphates.

There are two possible origins of the uniform chondrule-free

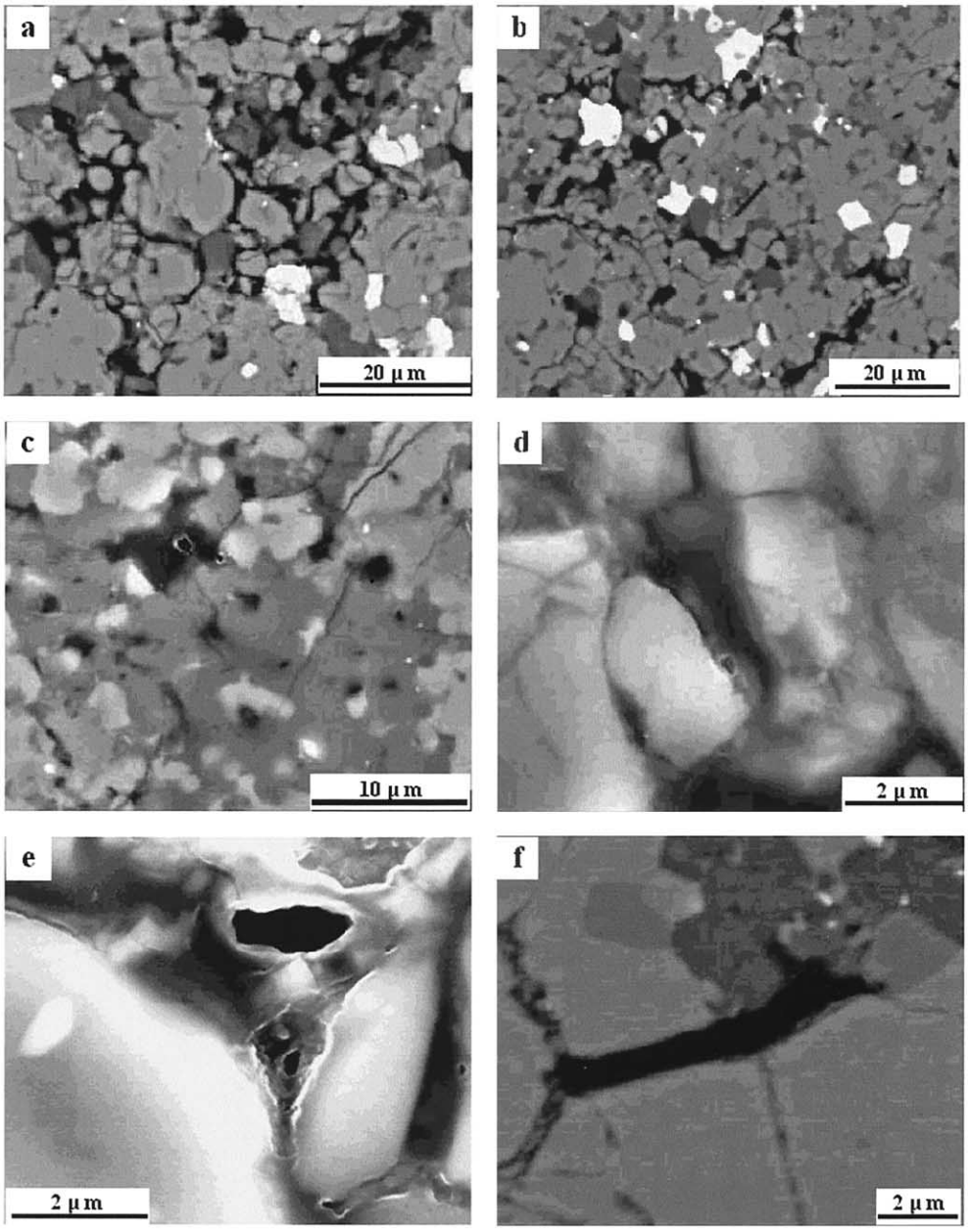

Fig. 7. BSE (a, f) and SE (b–e) images of C-rich material (black areas) within the fragments Gr7 (a–e) and Gr3 (f). Dark-grey—plagioclase mesostasis; grey—pyroxene; light-grey—olivine; white—troilite and metal. The Krymka polished sections. (a) Distribution of C-rich material within a plagioclase mesostasis. (b) Typical distribution of C-rich material and rare graphite crystals within the fragment Gr7. The C-rich material forms separate areas within a plagioclase mesostasis and intergranular veins. (c) A huge area of plagioclase mesostasis bearing C-rich material. (d) C-rich material within plagioclase mesostasis which contains a fine pore and exhibits plastic features of melted material. (e) Porous plagioclase mesostasis with C-rich material. (f) Transition of C-rich material located within plagioclase to graphite crystal.

textures with regular graphite crystals: crystallization from a melt containing carbon (Berkley and Jones, 1982; Treiman and Berkley, 1994; Rubin, 1997) or metamorphic processing of C-bearing precursor material (Buseck and Bo-Jun, 1985; Huss and Lewis, 1995; Luque et al., 1998). Our observations of the seven xenoliths allows us to conclude that graphite crystals are most likely the product of metamorphism of a fine-grained C-containing primary material. The main arguments for metamorphic processing of the xenolithic precursors are as follows:

1. The xenoliths do not exhibit any evidence of crystallization from a melt, especially from a shock melt. Their metal and sulfide particles are uniformly dispersed among silicates like those in other Krymka fragments composed of fine-grained material (Semenenko et al., 2001). During crystallization from a melt, metal and sulfide are mixed (like in enstatite chondrites or shock-melted chondritic material) and form coarse intergrown grains (Semenenko and Perron, 1995, 1996; Rubin, 1997); they are not to uniformly dispersed

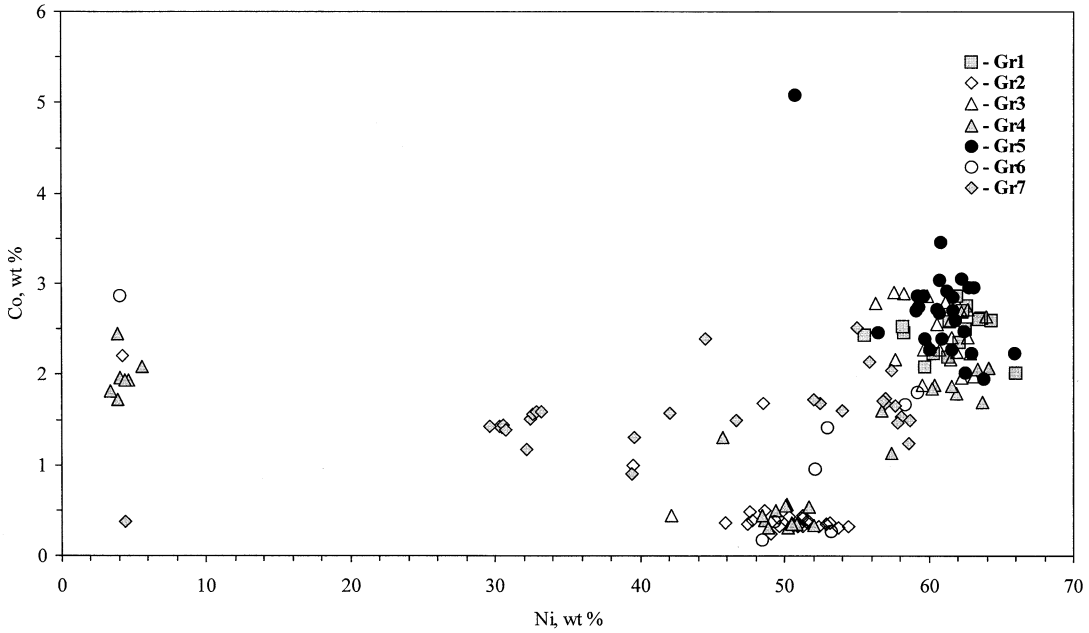

Fig. 8. Ni vs. Co plot of the metal particles within the graphite-containing fragments from Krymka.

within the xenoliths. The metal, sulfide and silicates do not show any structures of immiscible liquids, which are typical for shock melting (Begemann and Wlotska, 1969; Semenenko and Perron, 1995, 1996). In addition, rims of olivine grains within the xenoliths are not reduced like those in ureilites (Berkley et al., 1980; Treiman and Berkley, 1994).

2. In contrast to igneous graphite (Treiman and Berkley, 1994; Rubin 1997), the graphite within the xenoliths is nearly uniformly dispersed and predominantly restricted to interphase boundaries and in rare cases to silicate voids. With the exception of rare fine crystals, graphite crystals completely enclosed within silicates or spanning grain boundaries are absent. Most graphite crystals in the xenoliths are present as thin hexagonal plates, which appear as anomalous lamellae in polished sections, and do not show any other crystallographic forms. In addition the presence of pyramid pseudoforms on some graphite lamellae and a polycyclic growth of microcrystallites on the surface of one graphite crystal (Fig. 6b) are also indicative of metamorphic growth.
3. The xenoliths are similar to the Krymka carbonaceous clast K1 (Fig. 10) (Semenenko and Girich, 1996), which contains organic compounds (Semenenko et al., 1991a, 1991b; Semenenko, 1996). They represent a range of metamorphic varieties with different relationships between coarse and fine graphite crystals and C-rich material. Overall, there is a positive correlation between the abundance of graphite crystals and the metamorphic grade of the xenolithic material (a detailed discussion of this issue can be found below under “Genetic Relationships Between Graphite-Containing Fragments”).

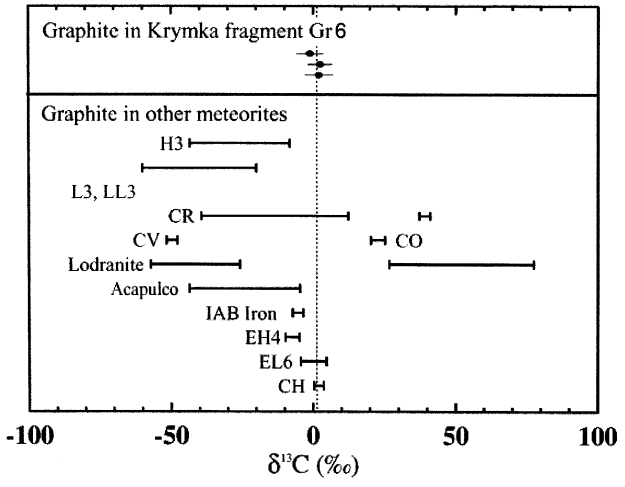

Fig. 9. C-isotopic composition of three graphite crystals from Krymka fragment Gr6 compared with ranges observed for graphite in other meteorites. Previous data are from El Goresy et al. (1995), Grady et al. (1996), Grady and Pillinger (1990), Mostefaoui et al. (1997, 2000), Newton et al. (1995), and Nittler and McCoy (2000).

Although the fragments have a recrystallized granular texture and relatively homogeneous silicate composition, they do preserve some evidence of their primary inhomogeneity. Some fragments (especially Gr7) are only partially recrystallized, contain a remarkable quantity of C-bearing material and a low amount of graphite crystals, and contain two chromite compositional groups (Appendix, Table A4), plagioclase and Ca-poor pyroxene (Appendix, Table A1). The record of primary inhomogeneity listed here may be explained by the accretional nature of the fragments. Should this be the case, the precursor of the recrystallized graphite-containing material had to be composed of two or three main constituents: inhomogeneous fine mineral grains, C-containing material, and probably chondrules. Though the absence of chondrules does not necessarily mean that the xenoliths were accreted in a chondrule-free

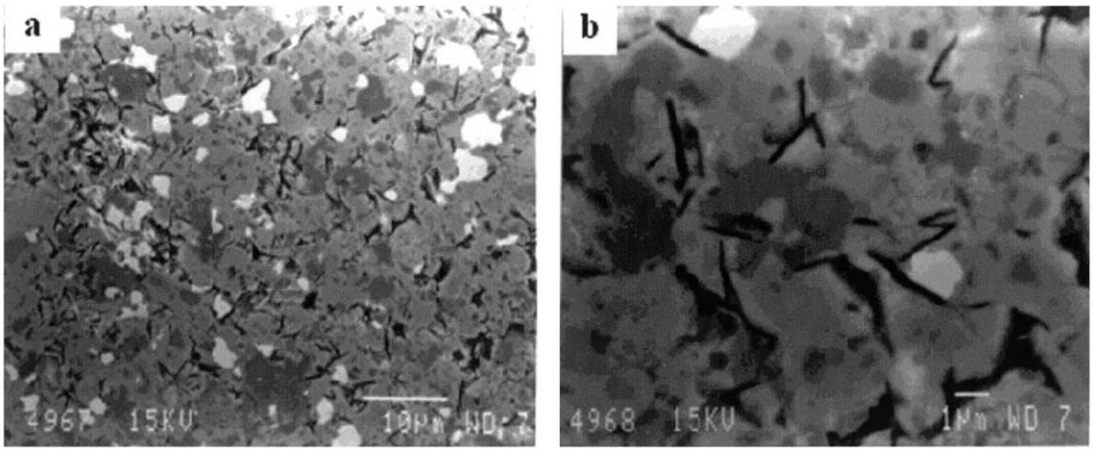

Fig. 10. BSE images of the carbonaceous clast K1 in the Krymka polished section. Black—graphite and C-rich material; dark-grey—plagioclase; grey—pyroxenes; light-grey—olivine; white—troilite and metal. (a) Distribution of fine graphite crystals (black lamellars) and C-rich material (black irregular areas) within the fragment. A texture of the fragment is finer-grained than that of the fragments Gr1 to Gr7. (b) Fine graphite crystals. Many of them form twins or triple junctures.

region of the solar nebula, the following features of the xenoliths have to be taken into account:

- Within seven xenoliths with a distinctive grade of metamorphism, not a single chondrule relic was found. The xenoliths are less processed (e.g., their silicates are not completely equilibrated) than equilibrated ordinary chondrites, which nevertheless bear chondrule relics.
- The xenoliths contain nearly uniformly distributed graphite crystals, attesting to a nearly uniform distribution of C-bearing precursor materials before metamorphism. Since chondrules are melted objects, they could not contain organic compounds, whereas primary fine-grained material could. If the xenoliths had formed by metamorphism of a C-bearing precursor with chondrules, they should exhibit graphite-free round areas with a diameter ~0.5 mm (based on the largest sizes of chondrules within the Krymka carbonaceous clasts K1; Semenenko et al., 1991a, 1991b). Such areas are absent within the xenoliths.
- In addition, it must be mentioned that some other Krymka fragments, composed of fine-grained material, are without chondrules (Semenenko et al., 2001): a few microchondrules were found in the fragment BK13, but none were found within the fine-grained material of BK14 although this material experienced a very low grade of metamorphism.

Taking all these data into account we suggest two possibilities: (1) a very low abundance of chondrules or microchondrules in the precursors of the xenoliths (like that inferred for the Krymka clast K1), which were obliterated during metamorphism; or (2) the absence of chondrules or microchondrules in the xenoliths precursors. The chemical and mineralogical similarity between the xenoliths and the carbonaceous clast K1, which is poor in chondrules and less metamorphically processed, allows us to identify the xenolith precursor materials as chondrule-poor. At the same time, we do not exclude the possibility that the precursors were in fact chondrule-free.

Accretion of inhomogeneous fine mineral grains, C-bearing material and probably chondrules or microchondrules in a chondrule-poor region of the solar nebula, followed by lithification, thermal metamorphism and collisional fragmentation are, from our point of view, the main processes likely to be responsible for the origin of the graphite-bearing fragments. They were subsequently accreted, together with typical unequilibrated ordinary chondrite material, ultimately to generate the Krymka parent body. At the same time, we do not exclude the possibility that the partial metamorphic processing of the xenoliths might have occurred as a result of a severe shock of Krymka itself.

4.1.2. Mineralogical distinctions

Mineralogical distinctions between the fragments and the host are most likely to be a result of differences in their primary compositions and preaccretionary evolutionary histories. The fragments are enriched in metal (2.2 vol.% in contrast to 0.9 vol.% in the host) and troilite (≥11.3 vol.% in contrast to 4.3 vol.% in the host), both of which are uniformly dispersed within graphite-containing material. In the host chondrite, metal and troilite are located within a fine-grained matrix as fine and coarse grains. Metallic minerals also have different compositions between the fragments and Krymka. The fragments contain awaruite, taenite and very rarely kamacite (Table 1; Appendix, Table A3), whereas the major metallic phase in the Krymka host is kamacite, with minor taenite with Ni <52 wt.% (Semenenko et al., 1987). The constant association of awaruite and taenite with troilite in the fragments suggests a genetic relationship. Paragenesis of metal with sulfide, a very low quantity of kamacite, high and correlated Ni and Co contents of the awaruite (Fig. 8), the cubic form of some sulfide crystals, which is common for metal but not for troilite, and the presence of metal relics within cubic troilite crystals are all evidence for troilite formation by metal sulfidization in an H_2S-rich environment (Semenenko and Girich, 1995). Considerable sulfidization of metal lowered its abundance and resulted in an increase in Ni and Co concentrations in the residual metal (Rambaldi and Wasson, 1980). Taking into account the total

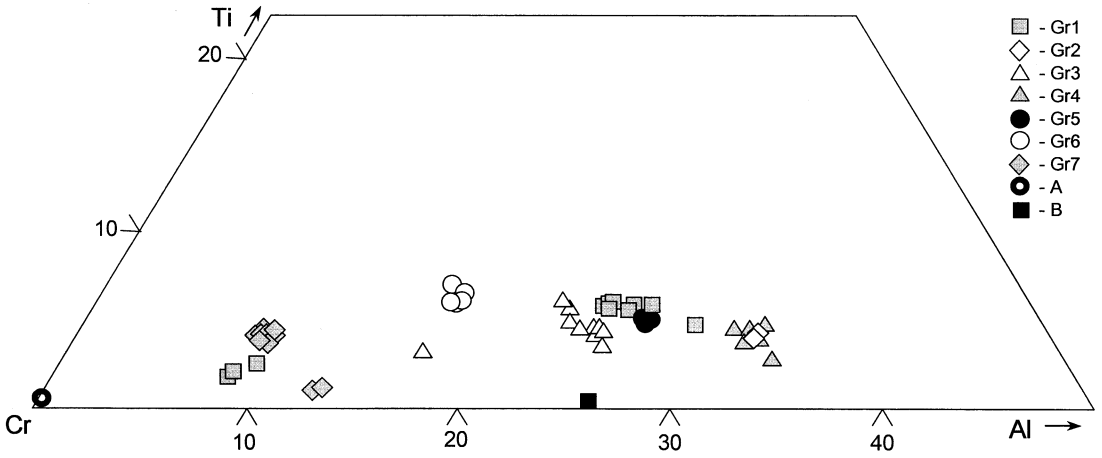

Fig. 11. Composition of chromite within the graphite-containing fragments from Krymka. (a, b) Two compositionally distinct chromites in the Krymka host from Bunch et al. (1967).

observed content of metal and sulfide particles, we may suppose that the precursor material of the fragments was enriched in metal.

Chromite in the fragments is enriched in TiO_2, Al_2O_3 and MgO (Appendix, Table A4), and differs from that of the host chondrite (Fig. 11). The Krymka host contains two compositional groups of chromite: group A—Al_2O_3-poor with 0.1 wt.% Al_2O_3, 0.4 wt.% MgO and 0.5 wt.% TiO_2; and group B—Al_2O_3-rich with 12.6 wt.% Al_2O_3, 8.4 wt.% MgO and 0.6 wt.% TiO_2 (Bunch et al., 1967). The Al_2O_3-rich group is only partially similar to chromites in the fragments in Al_2O_3-content. This indicates different primary composition and evolution trends. The high TiO_2-content in some chromites of the fragments corresponds to that of chromites of equilibrated LL-chondrites (Bunch et al., 1967) and may be considered as evidence of high-temperature formation (Matsjuk et al., 1989). However, it is not excluded that the TiO_2-rich chromites belong to relic grains formed in the nebula.

Another mineralogical peculiarity of the fragments (Semenenko and Girich, 1995) is the presence of F-apatite (Appendix, Table A2), which unlike Cl-apatite (van Schmus and Ribbe, 1969), is rare in meteorites but common in lunar (Frondel, 1978) and terrestrial igneous rocks (Fuchs, 1968). Fluorine has a very low abundance in ordinary chondrites, but it occurs in fluor-richterite in more reduced meteorites: enstatite chondrites, enstatite achondrites and iron meteorites (Bevan et al., 1977). The presence of F-apatite in the Orgueil (C1) chondrite was suggested by Jungck et al. (1981). The morphology of interstitial anhedral phosphate grains in the fragments attests to their metamorphic origin. It is possible that both the compositional features of phosphates and the high content of FeS are caused by the influence of hot fluids containing S, Cl and F during metamorphic processing of the fragments.

4.2. Relationship of the Xenoliths to Other Kinds of Material

The presence of euhedral graphite is the most important mineralogical feature of the fragments distinguishing them from the Krymka host and from other ordinary chondrites (Semenenko and Girich, 1995).

4.2.1. Mineralogical correspondences

The occurrence of euhedral graphite is not known in equilibrated ordinary chondrites and is very limited in unequilibrated ones. In addition, many peculiarities of the graphite crystals, including their morphologies, sizes, distribution and associations with other minerals, are different from those of any known kind of graphite-bearing cosmic material. Except for rare cases, crystalline graphite in the fragments (Fig. 5) is unlike the graphite in ureilites, enstatite and ordinary chondrites, iron meteorites and especially C-rich aggregates in unequilibrated chondrites. For example, graphite in enstatite chondrites is usually associated with metal and has a different morphology (Ramdohr, 1973). Graphite in most ureilites is poorly crystallized and is located within C-rich material (Berkley et al., 1980). Graphite in the Bishunpur chondrite (LL3) forms veins and small (<15 μm) rounded inclusions in association with metal (Mostefaoui et al., 2000). Graphite in iron meteorites occurs as globular inclusions within the metal (Mason, 1963). C-rich aggregates in ordinary chondrites consist of Fe-rich, micrometer and submicrometer sized poorly graphitized carbon grains (Lumpkin, 1986; Brearley et al., 1987), comprising clasts of matrix of unequilibrated chondrites which were classified as a new kind of type 3 chondrite (Scott et al., 1981a, 1981b). It is interesting that the size and morphology of the graphite (?) microcrystals from Gr1 (Semenenko and Girich, 1995) are similar to those of regular hexagonal plates of some solar system graphite grains chemically isolated from Murchison (CM2), but never observed in situ in chondrites (Amari et al., 1990; Zinner et al., 1990). As an exception, euhedral crystals of igneous graphite have been observed in some ureilites (Treiman and Berkley, 1994) and in enstatite chondrite impact-melt breccias (Rubin, 1997). However, the distribution, occurrence, and associations with other minerals of these graphite crystals and the mineralogy of their hosts are different from those of the graphite-bearing fragments studied here.

Of the known kinds of graphite-bearing meteoritic material, the fragments most closely correspond to the Krymka carbonaceous clast K1 (Fig. 10) (Semenenko and Girich, 1996). The latter contains fine graphite crystals, organic compounds and is enriched in volatiles (Semenenko et al., 1991a, 1991b; Semenenko, 1996). The sizes, morphology, occurrence and distribution of graphite within K1 are very similar to those of the fine graphite crystals from the studied fragments. Furthermore, the graphite abundance in K1 (≤4 vol.%) (Semenenko, 1996) is comparable with that of total graphite in Gr1. The distinctive features of the carbonaceous material in K1 are: (1) a higher FeO/(FeO + MgO) ratio (0.61); (2) the presence of chondrules and their clasts (although in low abundance); (3) a finer-granular texture (Fig. 10); (4) metal compositions typical of chondrites; (5) absence of coarse graphite crystals; (6) a higher inhomogeneity of silicates ($Fa_{22.0-45.7}$ and $Fs_{17.6-27.8}$); (7) the presence of organic compounds and enrichment in volatiles. The mineralogical and chemical differences between the studied fragments and K1 attest that the former experienced a higher level of metamorphic processing.

Thus, the mineralogy of the fragments Gr1 to Gr7 is similar to, but not identical with, that of the Krymka clast K1. We suggest that the precursors of all of these objects formed as a result of accretion of inhomogeneous minerals and C-containing material (most likely organic compounds) although the primary compositions of their primary minerals were different for the fragments and K1. In addition, the primary body of the graphite-bearing fragments experienced higher metamorphic alteration than that of the carbonaceous clast K1.

4.2.2. Chemical and isotopic correspondences

The approximate bulk compositions of the studied fragments, recalculated to 100%, allow us to make an approximation of their chemical resemblance to other kinds of meteoritic material. Their SiO_2/MgO ratio (~1.4) is similar to that of all classes of carbonaceous chondrites and is significantly lower than that observed in ordinary (~1.6) and enstatite (~1.85) chondrites (Jarosewich, 1990; Yanai and Kojima, 1995). The FeO/(FeO + MgO) ratio (0.51–0.59) is intermediate between that of ordinary chondrites (~0.3–0.43) and the carbonaceous clast K1 (0.62) supporting the mineralogical conclusion that the fragments are more recrystallized than K1. Moreover, the range of FeO/(FeO + MgO) ratios of the fragments overlaps that measured in several carbonaceous chondrites (Grossman et al., 1980, Jarosewich, 1990; Yanai and Kojima, 1995).

Unequilibrated ordinary chondrite falls have bulk C isotopic compositions that range from $\delta^{13}C = -28$ to –19‰ (Grady et al., 1989). Stepped combustion measurements of Krymka indicated a comparable range for subcomponents of the meteorite, with an average bulk composition of –21.8‰. The value of ~1‰ observed here for three graphite crystals from fragment Gr6 is thus considerably isotopically heavier than typical C in Krymka, further attesting to the exotic nature of the graphite-bearing fragments. Figure 9 shows the C isotopic composition of the Gr6 crystals, compared with ranges of $\delta^{13}C$ previously reported for graphite in several meteorite classes. Previous data for EH, EL and CH chondrites are based on stepped combustion measurements of bulk samples; all other data are ranges of ion probe measurements of individual graphite grains, in most cases associated with metal. Carbon in Gr6 graphite is isotopically heavier than that in metal-associated graphite in ordinary chondrites, but overlaps the ranges observed in EL6 chondrites (Grady et al., 1986), CH chondrites (Grady and Pillinger, 1990; Newton et al., 1995), the CR chondrite Acfer 182 (Mostefaoui et al., 1997), the acapulcoite Acapulco (El Goresy et al., 1995) and the lodranite Graves Nunataks 95209 (Nittler and McCoy, 2000). The large range of C isotopic compositions of graphite in primitive meteorites probably reflects a high level of heterogeneity in organic precursors in the solar nebula (Mostefaoui et al., 2000) and the distinct composition of the Krymka fragment likely does as well. The isotopic overlap of the graphite in the fragment with graphite from EL, CH, and CR chondrites, acapulcoites and lodranites suggests a possible relationship with the parent material of these meteorites. As discussed above, the bulk compositions of the fragments, especially the high SiO_2/MgO and FeO/(FeO + MgO) ratios, are much more similar to carbonaceous chondrites than to ordinary or enstatite chondrites. Thus, the chemical and isotopic data attest to a rather similar primary composition of the graphite-containing fragments and carbonaceous chondrites. Oxygen isotopic data for the graphite-bearing xenoliths would help make a firmer connection between the parental material of the fragments and specific meteorite classes.

The nitrogen contents of the three measured graphite crystals in Gr6 are much lower than those of graphites associated with metal in ordinary chondrites (Mostefauoi et al., 2000). Also, there was no evidence for large ^{15}N excesses observed sometimes in chondritic graphite. The low N abundance might indicate loss of N during the heating that caused the recrystallization of the fragments. However, graphite is a very retentive phase and graphite grains in the severely heated Acapulco meteorite have retained N (El Goresy et al., 1995). Thus, it appears to be more likely that the C-rich precursors to the graphite were *N*-poor.

4.3. Genetic Relationship Between Graphite-Containing Xenoliths

Although the studied fragments are mineralogically and chemically similar to each other, they differ in detail (Semenenko and Girich, 1998). For example, most features of Gr1 and Gr5 are similar except for some differences in the composition of F-apatite and chromite. Gr3 bears some resemblance to Gr1 and Gr5 but differs in having a higher Fa-content of olivine and in its lack of coarse crystals of graphite. Partial correspondence is observed for Gr2 and Gr4. They have nearly the same composition of silicates, chromite, taenite and kamacite. Gr6 and Gr7 are unlike each other and also differ from the rest of the fragments.

Despite the fact that we have only rough estimates of the bulk compositions of the fragments, differences in olivine composition as well as the variable presence of magnetite certainly point to different levels of oxidation of the fragments. These distinctions might be caused by some differences both in their primary composition and level of oxidation in a preaccretion period. The presence of magnetite in chondrites is of special interest, owing to the discussion about its cosmic or

terrestrial formation, especially in C-rich aggregates (Scott et al., 1981a, 1981b; Taylor et al., 1981; Brearley et al., 1987; Scott et al., 1988; Alexander et al., 1989). Fibrous magnetite has been observed in troilite of the Krymka matrix and has been interpreted as being formed by the oxidation of sulfide, and to have a preterrestrial origin (Alexander et al., 1989). Morphologically and compositionally, magnetite of the graphite-containing fragments corresponds to that of magnetite from the Krymka host. Many morphologic features indicate that the magnetite formed as a result of the replacement of troilite. Based on the mineralogy of Gr1, Semenenko and Girich (1995) gave preference to terrestrial replacement of troilite by magnetite, both in the fragments and in the host. However, of the seven studied graphite-containing fragments, only three bear magnetite and one has wüstite but not magnetite. Wüstite has been found in some dark, shocked chondrites (Eudin and Kolomensky, 1987) as product of shock transformation of metal or troilite. Since the fragments belong to an intensively shocked Krymka sample (Semenenko and Perron, 1995, 1996), we do not exclude the shock nature of the studied wüstite. This allows us to speculate a preterrestrial origin for both the magnetite and the wüstite in the fragments.

The main differences between the fragments are most likely caused by a range of metamorphic processing of their primary inhomogeneous precursor materials. This supposition is based on the differences of size and morphology of metamorphic minerals (chromite, plagioclase, phosphate and graphite), and compositional variations of the minerals. For example, chromite composition may be interpreted as a result of distinctions in their primary compositions and metamorphic alteration. Cr_2O_3, Al_2O_3, TiO_2, MgO and FeO are the most variable components of the chromites (Appendix, Table A4). There are five compositional groups of chromites (Fig. 11). Four of them are within one isomorphous sequence $Cr_2O_4^{2-}$–$Al_2O_4^{2-}$ (Fig. 12), that testifies to a genetic relationship. The composition of the chromite is also variable within the groups, in Cr_2O_3, TiO_2 and less so in Al_2O_3 and MgO and (Fig. 12).

A correlation of the atomic ratios $Fe^{2+}/(Fe^{2+} + Mg)$ and $Cr/(Cr + Al)$ shows a minimum of two crystallization trends (Fig. 13), which are common between chromites from all the fragments except Gr6. At the same time, each of the fragments has its own small trend of compositional evolution of the chromite. These data attest to a multistage process of chromite formation, based probably on a heterogeneous nature of the chromites and different degrees of metamorphic alteration of the fragments.

Differences in size of the graphite crystals between fragments may also be explained by distinct metamorphic histories. There is some tendency towards a reverse correlation between the quantity of large graphite crystals and the presence of C-rich material. For example, Gr7, which contains only fine graphite crystals without any large ones, is enriched in C-rich material. The observable transition of this material into fine graphite crystals (Fig. 7f) supports a genetic relationship. The foregoing and data on metamorphic conversion of carbonaceous material to graphite (Buseck and Bo-Jun, 1985) allow us to speculate that the fragments with a predominance of fine graphite crystals and C-rich material experienced a lower grade of metamorphic processing than those with abundant large graphite crystals.

Unfortunately, we do not have detailed data on the structure and composition of the C-rich material. This material is associated predominantly with plagioclase mesostasis (Fig. 7). Some morphologic features of the C-rich material (such as rare shrinkage cracks, the presence of C-rich veins and its arrangement along phase boundaries and fractures; Figs. 7a and 7b) indicate heating and sharp cooling, most probably caused by shock metamorphism. The latter features indicate that the C-rich material has a low melting point and is mobile. The melting point has to be the same as or lower than that of the feldspathic mesostasis. Carbon-rich mesostasis also contains pores (Figs. 7c–7e) that may be due to mobilization of gas from precursors (organic compounds?) conceivably as a result of shock metamorphism.

There are two ways graphite typically forms in nature (see review by Luque et al., 1998): (1) the heating and compression of organic matter in situ, i.e., as a result of metamorphism; (2) the precipitation of solid carbon (graphite) from CO_2-, $CO-$, and/or CH_4- containing fluids. The mineralogical and chemical features of the graphite bearing fragments point to the former method. Based on the unequilibrated nature of the precursor material of the fragments and its resemblance to carbonaceous chondrites we speculate that thermal metamorphism caused the following transformations of a primary C-containing material: probably organic compounds → C-rich material → fine crystals of graphite → large crystals of graphite. Although many of the structural and chemical features of this material have yet to be studied in detail, the proposed scheme of metamorphic formation of the graphite seems to be the most probable.

4.4. Post Accretional Features of the Xenoliths

After accretion, the Krymka parent body experienced shock metamorphism as a result of a minimum of two shocks in situ. The first of these caused formation of the shock-melted portions of the chondritic material and was much more intensive (shock up to 75–90 GPa in case of nonporous primary material and 30 GPa in porous material, and shock heating up to 1500°C) than the following one, which caused only deformation of the minerals (Semenenko and Girich, 1995; Semenenko and Perron, 1995, 1996).

The graphite-containing fragments show effects (Figs. 1d, 7a, and 7b) of a less intensive shock than the rest of the sample N 1290/29. In view of the limited number of olivine grains studied in transmitted light, we are not able to estimate the shock pressure inside the fragments. Among the fragments, Gr4 experienced the highest shock heating. The presence of melt structures of troilite within the fragment indicates shock heating up to 988°C. The veins of carbon rich material in Gr7 were probably formed at lower temperature.

Taking into account the fact that the seven graphite-bearing fragments are present within a Krymka sample that was shocked more intensively than the rest of the chondrite, we suppose that this shock might be responsible for the partial metamorphic processing of the xenoliths. This supposition is supported by the following mineralogical details: (1) The fragments and the carbonaceous clast K1 are found in different Krymka samples and exhibit a correlation between evidence of thermal metamorphism within the xenoliths and shock effects

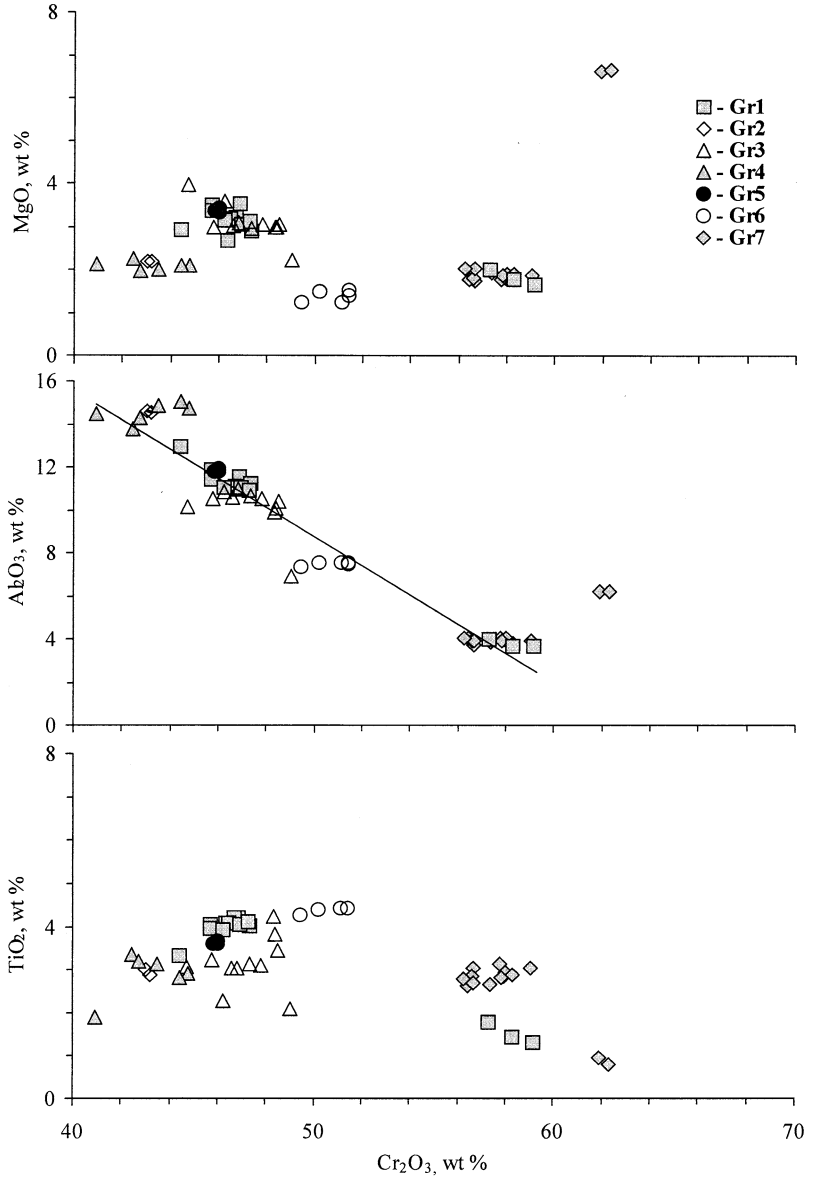

Fig. 12. MgO, Al_2O_3 and TiO_2 vs. Cr_2O_3 of chromites within the fragments Gr1 to Gr7 from Krymka.

within the xenolith-bearing chondritic samples. (2) Fine-grained accretional rims of Gr1 to Gr7 are partially recrystallized, in contrast to that of the clast K1, indicating that they were thermally metamorphosed within the Krymka parent body.

5. CONCLUSIONS

Seven graphite-containing xenoliths, which are distinct from any known kind of meteoritic material, were found within one sample of the Krymka chondrite. Mineralogically, the xenoliths are similar, but not identical, to the Krymka carbonaceous clast K1, which bears graphite microcrystals, organic compounds and is enriched in volatiles. Chemically and isotopically, they most closely resemble carbonaceous chondrites. The mineralogical, chemical and isotopic data for the graphite-containing fragments allows us to propose:

1. The xenoliths were accreted with typical chondritic material (chondrules, fine-grained matrix and xenoliths) as collisional fragments of a primary rock (or rocks).
2. The primary rock (rocks) of the xenoliths was formed as a result of accretion of two or three main constituents—fine-grained inhomogeneous minerals, carbon-containing material (most likely organic compounds) and probably chondrules or microchondrules, in a chondrule-poor region of the solar nebula. Subsequent lithification and thermal metamorphism caused textural and compositional processing of the primary material. The metamorphic alteration of the carbon-containing material could have been caused by the lithifi-

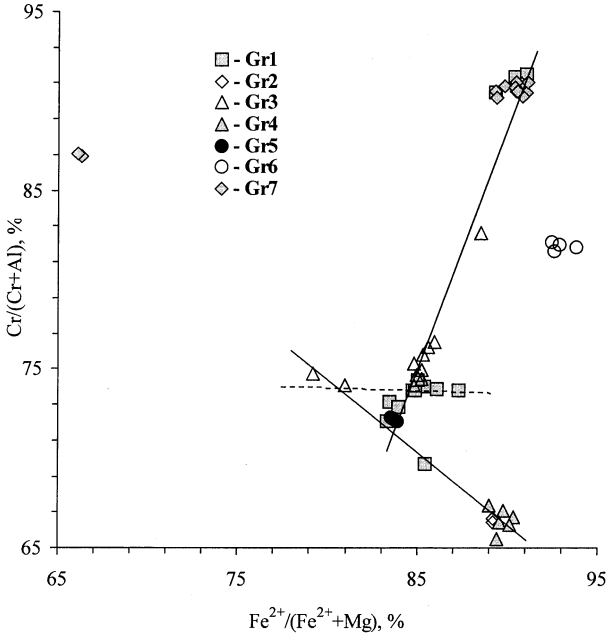

Fig. 13. A correlation of atomic ratios $Fe^{2+}/(Fe^{2+} + Mg)$ and $Cr/(Cr + Al)$ of chromites within the graphite-containing fragments from Krymka.

cation of the primary body and/or an intensive shock of the Krymka parent body.

3. The graphite-containing materials represent metamorphosed varieties of a previously unknown type of unequilibrated carbonaceous matter. Most likely, the graphite has a metamorphic nature and was crystallized from C-containing precursors through the following sequence: probably organic compounds → C-rich material → graphite.

Acknowledgments—This work was supported by Smithsonian Institution grant (Ng50208) and partially by the grants of INTAS (93-2101) and of the German Research Foundation (GRK 189/3, 436UKR 113/51/0-1). We thank T. Grund for technical assistance, and T. Koromyslichenko, F. Bartschat, N. Kiriljuk and I. Kvasnitsa for help with the preparation of the manuscript. We are grateful to E. Jarosewich, G. MacPherson, S. Russell, E. Sobotovich, C. Perron, E. Jessberger, A. Bischoff, S. Matsjuk and V. Kvasnitsa for kind supporting of this work and for helpful discussions. We also thank Smail Mostefaoui, two anonymous reviewers and Monica Grady for thoughtful reviews that significantly improved the manuscript.

Associate editor: M. Grady

REFERENCES

Alexander C. M. O., Hutchison R., and Barber D. J. (1989) Origin of chondrule rims and interchondrule matrices in unequilibrated ordinary chondrites. *Earth Planet. Sci. Lett.* **95,** 187–207.

Amari S., Anders E., Virag A., and Zinner E. (1990) Interstellar graphite in meteorites. *Nature* **345,** 238–240.

Begemann F. and Wlotska F. (1969) Shock induced thermal metamorphism and mechanical deformations in the Ramsdorf chondrite. *Geochim. Cosmochim. Acta* **33,** 1351–1370.

Berkley J. L. and Jones J. H. (1982) Primary igneous carbon in ureilites: Petrological implications [abstract]. *Lunar Planet. Sci.* **13,** 353–364.

Berkley J. L., Taylor G., and Keil K. (1980) The nature and origin of ureilites. *Geochim. Cosmochim. Acta* **44,** 1579–1597.

Bevan A. W. R., Bevan J. C., and Francis J. G. (1977) Amphibole in the Mayo Belwa meteorite: First occurrence in an enstatite achondrite. *Mineral. Mag.* **41,** 531–534.

Brearley A. J., Scott E. R. D., and Keil K. (1987) Carbon-rich aggregates in ordinary chondrites: Transmission electron microscope observations of Sharps (H3) and Plainview (H regolith breccia). *Meteoritics* **22,** 338–339.

Bunch T. E., Keil K., and Snetsinger K. G. (1967) Chromite composition in relation to chemistry and texture of chondrites. *Geochim. Cosmochim. Acta* **31,** 1569–1582.

Buseck P. R. and Bo-Jun H. (1985) Conversion of carbonaceous material to graphite during metamorphism. *Geochim. Cosmochim. Acta* **49,** 2003–2016.

El Goresy A., Zinner E., and Marti K. (1995) Survival of isotopically heterogeneous graphite in a differentiated meteorite. *Nature* **373,** 469–499.

Endress M., Keil K., Bischoff A., Spettel B., Clayton R. N., and Mayeda T. K. (1994) Origin of dark clasts in the Acfer 059/E1 Djouf 001 CR2 chondrite. *Meteoritics* **29,** 26–40.

Eudin I. A. and Kolomensky V. D. (1987) *Mineralogy of Meteorites* [in Russian]. Sverdlovsk.

Fodor R. V. and Keil K. (1978) *Catalog of Lithic Fragments in LL-Group Chondrites*. University of New Mexico, Institute of Meteoritics, Albuquerque.

Frondel J. W. (1978) *Lunar Mineralogy* [in Russian]. Mir, Moscow.

Fuchs L. H. (1968) The phosphate mineralogy of meteorites. In *Meteorite Research* (ed. P. M. Millman), pp. 683–695. Springer-Verlag, New York.

Grady M. M. and Pillinger C. T. (1990) ALH85085: Nitrogen isotope analysis of a highly unusual primitive chondrite. *Earth Planet. Sci. Lett.* **97,** 29–40.

Grady M. M., Wright I. P., Carr L. P., and Pillinger C. T. (1986) Compositional differences in enstatite chondrites based on carbon and nitrogen stable isotope measurements. *Geochim. Cosmochim. Acta* **50,** 2799–2813.

Grady M. M., Wright I. P., and Pillinger C. T. (1989) A preliminary investigation into the nature of carbonaceous material in ordinary chondrites. *Meteoritics* **24,** 147–154.

Grossman L., Allen J. M., and MacPherson G. J. (1980) Electron microprobe study of a "mysterite"-bearing inclusion from the Krymka LL-chondrite. *Geochim. Cosmochim. Acta* **44,** 211–216.

Huss G. R. (1979) *The Matrix of Unequilibrated Ordinary Chondrites: Implications for the Origin and History of Chondrites*. Master's thesis, University of New Mexico.

Huss G. R. and Lewis R. S. (1995) Presolar diamond, SiC, and graphite in primitive chondrites: Abundances as a function of meteorite class and petrologic type. *Geochim. Cosmochim. Acta* **59,** 115–160.

Jarosewich E. (1990) Chemical analyses of meteorites—A compilation of stony and iron meteorite analyses. *Meteoritics* **25,** 323–337.

Jungck M. H. A., Meier F. O., and Eberhardt P. (1981) Apatite in Orgueil. Carrier phase for neon-E? *Meteoritics* **16,** 336–337.

Keil K. and Fredriksson K. (1964) The iron, magnesium and calcium distribution in coexisting olivines and rhombic pyroxenes of chondrites. *J. Geophys. Res.* **69,** 3487–3515.

Kurat G. (1970) Zur Genese des kohligen Materials in Meteoriten von Tieschitz. *Earth Planet. Sci. Lett.* **7,** 317–324.

Lumpkin G. R. (1986) High resolution electron microscopy of carbonaceous material from CI, CM, CV and H chondrites [abstract]. *Lunar Planet. Sci.* **17,** 502–503.

Luque F. J., Pasteris J. D., Wopenka B., Rodas M., and Barrenechea J. F. (1998) Natural fluid-deposited graphite: Mineralogical characteristics and mechanisms of formation. *Am. J. Sci.* **298,** 471–498.

Mason B. (1963) *Meteorites*. John Wiley, New York.

Matsjuk S. S., Platonov A. N., Polshin E. V., Taran M. N., Tatarintsev V. I., Badion N. S., Vishnevsky A. A., Safronov A. F., and Smirnov G. I. (1989) *Spinels of Mantle Rocks* [in Russian]. Naukova Dumka, Kyiv, Ukraine.

Mostefaoui S., Zinner E., Hoppe P. and El Goresy A. (1997) In situ survey of graphite in unequilibrated chondrites—Morphologies, C, N and H isotopes [abstract]. *Lunar Planet. Sci.* **28,** #989.

Mostefaoui S., Perron C., Zinner E., and Sagon G. (2000) Metal-associated carbon in primitive chondrites: Structure, isotopic composition, and origin. *Geochim. Cosmochim. Acta* **64,** 1945–1964.

Nelson V. E. and Rubin A. E. (2002) Size-frequency distributions of chondrules and chondrule fragments in LL3 chondrites: Implications for parent-body fragmentation of chondrules. *Meteorit. Planet. Sci.* **37,** 1361–1376.

Newton J., Grady M. M., and Pillinger C. T. (1995) A new member of the "CH" chondrite group of meteorites: Nitrogen and carbon stable isotope geochemistry of RKP 92435 [abstract]. *Lunar Planet. Sci.* **26,** 1045–1046.

Nittler L. R. and McCoy T. J. (2000) Carbon isotopes in graphite from lodranite Graves Nunataks 95209. *Meteorit. Planet. Sci.* **35,** A120.

Rambaldi E. R. and Wasson J. T. (1980) The origin of chondrule rims in the Bishunpur (L3) chondrite. *Meteoritics* **15,** 352.

Ramdohr P. (1973) *The Opaque Minerals in Stony Meteorites*. Elsevier, Berlin.

Rubin A. E. (1997) Igneous graphite in enstatite chondrites. *Mineral. Mag.* **61,** 699–703.

Scott E. R. D., Rubin A. E., Taylor G. J., and Keil K. (1981a) New kind of type 3 chondrite with a graphite-magnetite matrix. *Earth Planet. Sci. Lett.* **56,** 19–31.

Scott E. R. D., Taylor G. J., Rubin A. E., Okada A., and Keil K. (1981b) Graphite-magnetite aggregates in ordinary chondritic meteorites. *Nature* **291,** 544–546.

Scott E. R. D., Brearley A. J., Keil K., Grady M. M., Pillinger C. T., Clayton R. N., Mayeda T. K., Wieler R., and Signer P. (1988) Nature and origin of C-rich ordinary chondrites and chondritic clasts [abstract]. *Lunar Planet. Sci.* **18,** 513–523.

Semenenko V. P. (1996) New data on a carbonaceous clast in the Krymka chondrite. *Meteorit. Planet. Sci.* **31,** A126–A127.

Semenenko V. P. and Girich A. L. (1995) Mineralogy of a unique graphite-containing fragment in the Krymka chondrite (LL3). *Mineral. Mag.* **59,** 445–456.

Semenenko V. P. and Girich A. L. (1996) Graphite-containing fragments in the Krymka chondrite. *Meteorit. Planet. Sci.* **31,** A127.

Semenenko V. P. and Girich A. L. (1998) The nature of graphite-containing fragments in the Krymka (LL3) chondrite. *Meteorit. Planet. Sci.* **33,** A141.

Semenenko V. P. and Girich A. L. (2001) A variety of lithic fragments in the Krymka (LL3.1) chondrite. *Meteorit. Planet. Sci.* **36,** A187.

Semenenko V. P. and Perron C. (1995) Shock-melted regions in the Krymka (LL3) chondrite. *Meteoritics* **30,** 577.

Semenenko V. P. and Perron C. (1996) Shock-melted regions in the Krymka chondrite (LL3) [in Russian]. *Mineral. J.* **18 (*4*),** 26–37.

Semenenko V. P., Sobotovich E. V., and Tertichnaya B. V. (1987) *Meteorites of Ukraine* [in Russian]. Naukova Dumka, Kyiv, Ukraine.

Semenenko V. P., Kolesov G. M., Samoilovich L. G., Golovko N. V., Ljul A. Yu, and Kovaljuh N. N. (1991a) Carbonaceous inclusions in the Krymka (LL3) chondrite [in Russian]. *Geokhimiya* **8,** 1111–1121.

Semenenko V. P., Kolesov G. M., Samoilovich L. G., Golovko N. V., and Ljul A. Yu. (1991b) Carbonaceous inclusions in the Krymka (LL3) chondrite [abstract]. *Lunar Planet. Sci.* **22,** 1213–1214.

Semenenko V. P., Nittler L. R., and Girich A. L. (1998) The Krymka chondrite (LL3): A graphite-containing fragment and isotopic composition of its graphite crystals. *Meteorit. Planet. Sci.* **33,** A141–A142.

Semenenko V. P., Bischoff A., Weber I., Perron C., and Girich A. L. (2001) Mineralogy of fine-grained material in the Krymka (LL3.1) chondrite. *Meteorit. Planet. Sci.* **36,** 1067–1085.

Taylor G. J., Okada A., Scott E. R. D., Rubin A. E., Huss G. R., and Keil K. (1981) The occurrence and implications of carbide-magnetite assemblages in unequilibrated ordinary chondritis [abstract]. *Lunar Planet. Sci.* **12,** 1076–1078.

Treiman A. H. and Berkley J. L. (1994) Igneous petrology of the new ureilites Nova 001 and Nullarbor 010. *Meteoritics* **29,** 843–848.

Van Schmus W. R. and Ribbe P. H. (1969) Composition of phosphate minerals in ordinary chondrites. *Geochim. Cosmochim. Acta* **33,** 637–640.

Van Schmus W. R. and Wood J. A. (1967) A chemical-petrologic classification for the chondritic meteorites. *Geochim. Cosmochim. Acta* **31,** 745–765.

Wlotzka F. (1983) Composition of chondrules, fragments and matrix in the unequilibrated ordinary chondrites Tieschitz and Sharps. In *Chondrules and Their Origins* (ed. E. A. King), pp. 296–318. Lunar and Planetary Institute, Houston, TX.

Yanai K. and Kojima H. (1995) *Catalog of the Antarctic Meteorites*. National Institute of Polar Research, Tokyo.

Zinner E., Wopenka B., Amari S., and Anders E. (1990) Interstellar graphite and other carbonaceous grains from the Murchison meteorite: Structure, composition and isotopes of C, N and Ne [abstract]. *Lunar Planet. Sci.* **21,** 1379–1380.

Zinner E., Amari S., Wopenka B., and Lewis R. S. (1995) Interstellar graphite in meteorites: Isotopic compositions and structural properties of single graphite grains from Murchison. *Meteoritics* **30,** 209–226.

Table A1. Electron microprobe analyses (wt.%) of silicates within the graphite-containing xenoliths from Krymka.

	Gr1		Gr2		Gr3		Gr4		Gr5		Gr6		Gr7		
Olivine	Mean (50)	SD	Mean (57)	SD	Mean (47)	SD	Mean (98)	SD	Mean (35)	SD	Mean (93)	SD	Mean (82)	SD	
SiO_2	37.0	*0.7*	36.9	*1.0*	36.1	*0.5*	37.0	*0.5*	35.9	*0.4*	38.2	*0.5*	37.6	*0.5*	
Al_2O_3	<0.01	*0.02*	0.09	*0.15*	0.07	*0.11*	<0.02	*0.03*	0.11	*0.14*	<0.01	*0.02*	<0.02	*0.03*	
MgO	34.6	*1.8*	35.4	*0.9*	30.6	*0.5*	33.6	*0.9*	34.0	*0.9*	38.2	*0.4*	34.3	*0.6*	
TiO_2	<0.02	*0.03*	<0.02	*0.02*	<0.02	*0.02*	<0.02	*0.02*	<0.02	*0.02*	<0.02	*0.02*	<0.02	*0.02*	
CaO	0.07	*0.09*	0.10	*0.08*	0.04	*0.02*	0.08	*0.03*	0.10	*0.29*	0.10	*0.02*	0.04	*0.04*	
FeO	27.9	*1.9*	26.6	*1.2*	32.2	*0.8*	29.2	*1.1*	28.5	*1.0*	23.5	*0.6*	28.2	*0.6*	
MnO	0.29	*0.07*	0.34	*0.07*	0.42	*0.06*	0.30	*0.05*	0.33	*0.05*	0.43	*0.06*	0.44	*0.06*	
Cr_2O_3	0.05	*0.06*	0.09	*0.18*	0.06	*0.04*	0.05	*0.05*	0.07	*0.05*	0.08	*0.05*	0.05	*0.04*	
P_2O_5	0.06	*0.13*	0.06	*0.08*	0.05	*0.07*	0.06	*0.05*	0.05	*0.05*	<0.03	*0.04*	0.04	*0.04*	
Total	100.05	*1.0*	99.53	*1.1*	99.67	*0.8*	100.46	*0.8*	99.21	*0.7*	100.57	*0.8*	100.75	*0.6*	
Fa	31.2	*2.5*	29.6	*1.3*	37.1	*0.8*	32.8	*1.3*	32.0	*1.2*	25.6	*0.6*	31.5	*0.8*	
Ca-poor pyroxene															
	Mean (6)	*SD*	Mean (19)	*SD*	Mean (24)	*SD*	Mean (38)	*SD*	Mean (10)	*SD*	Mean (73)	*SD*	Mean (7)	*SD*	1 analysis
SiO_2	54.2	*1.8*	54.3	*2.2*	54.0	*1.1*	54.4	*1.3*	52.8	*1.6*	55.2	*0.6*	55.90	*0.83*	57.97
Al_2O_3	0.42	*0.10*	0.56	*0.13*	0.44	*0.24*	0.60	*0.16*	0.50	*0.06*	0.29	*0.03*	0.18	*0.06*	0.47
MgO	28.4	*1.2*	27.8	*0.7*	27.6	*0.6*	27.6	*0.7*	27.9	*1.2*	28.3	*0.2*	28.10	*1.56*	36.18
TiO_2	0.17	*0.04*	0.17	*0.03*	0.15	*0.07*	0.18	*0.05*	0.20	*0.06*	0.22	*0.04*	0.12	*0.04*	0.04
CaO	0.79	*0.17*	0.68	*0.14*	0.83	*0.36*	0.88	*0.54*	1.15	*1.26*	1.12	*0.07*	1.00	*0.79*	0.39
FeO	15.6	*1.6*	15.4	*1.3*	15.4	*0.5*	15.5	*1.1*	15.7	*0.9*	14.2	*0.5*	15.07	*3.13*	3.21
MnO	0.35	*0.06*	0.37	*0.07*	0.42	*0.05*	0.38	*0.06*	0.39	*0.06*	0.43	*0.07*	0.51	*0.30*	0.26
Cr_2O_3	0.23	*0.08*	0.20	*0.03*	0.24	*0.58*	0.25	*0.12*	0.23	*0.04*	0.24	*0.03*	0.24	*0.32*	0.70
P_2O_5	0.05	*0.09*	0.06	*0.07*	<0.02	*0.06*	<0.03	*0.07*	0.04	*0.06*	<0.01	*0.02*	<0.01	*0.01*	<0.01
V_2O_3	n.a.	—	<0.02	*0.02*	<0.03	*0.03*	<0.01	*0.02*	<0.03	*0.05*	<0.01	*0.01*	n.d.	—	<0.02
Na_2O	0.06	*0.03*	0.04	*0.05*	0.06	*0.06*	0.05	*0.04*	0.06	*0.04*	<0.03	*0.02*	0.05	*0.06*	0.08
Total	100.37	*1.1*	99.68	*1.0*	99.20	*1.1*	99.99	*0.8*	99.11	*0.7*	100.20	*0.7*	101.19	*0.69*	99.41
Fs	23.2	*1.6*	23.4	*1.5*	23.4	*0.8*	23.6	*1.5*	23.5	*1.0*	21.5	*0.7*	22.66	*4.66*	4.71
En	75.3	*1.6*	75.3	*1.4*	75.0	*0.8*	74.7	*1.3*	74.3	*3.1*	76.3	*0.7*	75.40	*4.42*	94.55
Wo	1.52	*0.4*	1.32	*0.3*	1.62	*0.7*	1.72	*1.1*	2.19	*2.4*	2.17	*0.1*	1.94	*1.53*	0.74
Ca-rich pyroxene															
	Mean (6)	*SD*	Mean (9)	*SD*	Mean (12)	*SD*	Mean (53)	*SD*	Mean (4)	*SD*	Mean (16)	*SD*	Mean (3)		
SiO_2	53.5	*1.6*	53.2	*1.7*	52.5	*0.6*	52.9	*0.9*	51.1	*3.6*	53.5	*0.5*	53.2		
Al_2O_3	1.54	*0.7*	1.94	*0.9*	1.16	*0.1*	1.82	*0.3*	1.79	*1.2*	0.63	*0.05*	0.73		
MgO	15.8	*0.5*	15.6	*1.0*	15.6	*0.5*	15.5	*0.9*	16.8	*3.3*	16.2	*0.3*	16.5		
TiO_2	0.53	*0.06*	0.53	*0.12*	0.36	*0.08*	0.55	*0.09*	0.47	*0.11*	0.56	*0.08*	0.31		
CaO	20.6	*0.9*	19.7	*3.2*	21.9	*0.5*	20.6	*1.6*	18.8	*4.9*	21.6	*0.4*	22.1		
FeO	6.57	*1.5*	6.89	*2.6*	5.84	*0.8*	6.09	*1.3*	8.53	*5.5*	5.80	*0.3*	5.53		
MnO	0.15	*0.08*	0.19	*0.06*	0.17	*0.03*	0.19	*0.06*	0.17	*0.06*	0.20	*0.05*	0.18		
Cr_2O_3	0.71	*0.13*	0.92	*0.29*	0.68	*0.08*	0.89	*0.13*	0.72	*0.14*	0.67	*0.07*	0.54		
P_2O_5	0.07	*0.05*	0.28	*0.54*	0.04	*0.07*	0.03	*0.05*	0.04	*0.04*	<0.01	*0.02*	0.07		
V_2O_3	n.a.	—	0.09	*0.05*	n.a.	—	0.07	*0.02*	0.05	*0.06*	0.05	*0.02*	<0.03		
Na_2O	0.78	*0.07*	1.04	*0.4*	0.65	*0.09*	0.99	*0.17*	0.94	*0.48*	0.46	*0.04*	0.49		
Total	100.16	*1.0*	100.35	*1.1*	98.92	*0.9*	99.81	*0.6*	99.48	*1.0*	99.79	*0.6*	99.79		
Fs	10.7	*2.1*	11.5	*4.4*	9.46	*1.2*	10.1	*2.0*	13.2	*7.0*	9.30	*0.5*	8.73		
En	46.0	*1.3*	46.5	*3.0*	45.1	*0.9*	46.0	*2.0*	47.5	*5.1*	46.3	*0.8*	46.5		
Wo	43.2	*2.3*	42.0	*6.7*	45.4	*1.1*	43.9	*3.8*	39.3	*12.0*	44.4	*0.9*	44.8		
Feldspatic plagioclase															
	Mean (5)	*SD*	Mean (2)		Mean (2)		1 analysis		Mean (6)	*SD*	Mean (14)	*SD*	Mean (7)	*SD*	1 analysis
SiO_2	63.1	*1.2*	61.6		62.3		61.3		62.7	*1.1*	63.2	*0.6*	66.45	*0.80*	45.78
Al_2O_3	22.1	*0.7*	21.4		22.1		21.5		22.9	*0.5*	22.4	*0.2*	20.27	*0.32*	32.15
MgO	0.45	*0.38*	0.40		0.21		1.02		0.15	*0.10*	0.05	*0.04*	0.19	*0.28*	0.71
TiO_2	0.06	*0.04*	0.04		0.04		<0.03		<0.03	*0.04*	0.05	*0.03*	<0.01	*0.01*	0.05
CaO	3.53	*0.1*	3.56		3.42		3.50		3.77	*0.1*	3.88	*0.1*	1.26	*0.17*	16.14
FeO	1.29	*0.3*	2.18		1.45		1.45		0.88	*0.05*	0.88	*0.08*	1.04	*0.10*	1.84
MnO	<0.01	*0.02*	<0.01		0.04		0.04		<0.01	*0.01*	<0.02	*0.02*	<0.02	*0.03*	n.d.
Cr_2O_3	<0.03	*0.03*	0.06		<0.02		n.d.		<0.02	*0.03*	<0.02	*0.02*	<0.02	*0.02*	<0.03
P_2O_5	0.08	*0.08*	0.07		0.06		0.75		<0.03	*0.02*	<0.01	*0.01*	0.06	*0.09*	<0.01
Na_2O	9.32	*0.45*	8.63		8.40		9.51		9.14	*0.1*	9.21	*0.3*	9.96	*1.10*	1.59
K_2O	0.06	*0.03*	<0.02		0.09		0.13		0.04	*0.02*	<0.02	*0.03*	0.53	*0.06*	0.04
Total	100.05	*1.5*	97.98		98.13		99.18		99.72	*1.4*	99.76	*0.89*	99.81	*1.18*	98.31
Ab	82.4	*0.9*	81.3		81.1		82.5		81.2	*0.6*	81.0	*0.4*	90.45	*1.10*	15.09
An	17.3	*1.0*	18.5		18.3		16.8		18.5	*0.7*	18.9	*0.5*	6.36	*0.82*	84.65
Or	0.36	*0.15*	0.15		0.61		0.74		0.23	*0.13*	0.11	*0.16*	3.19	*0.63*	0.26

The number of analyses is given in parentheses.
SD = standard deviation; n.a. = not analyzed; n.d. = not detected.

Table A2. Electron microprobe analyses (wt.%) of phosphates within the graphite-containing xenoliths from Krymka.

	Gr1	Gr2		Gr3		Gr4	Gr5		Gr6		Gr7	
Apatite	1 analysis	Mean (5)	SD	Mean (6)	SD		Mean (3)		Mean (4)	SD	Mean (9)	SD
SiO_2	0.45	0.32	*0.26*	0.88	*0.67*		0.33		1.01	*0.7*	0.59	*0.53*
Al_2O_3	0.14	0.08	*0.07*	0.05	*0.06*		<0.03		0.11	*0.07*	0.11	*0.10*
MgO	0.18	0.15	*0.14*	0.71	*0.39*		0.64		0.44	*0.41*	0.29	*0.19*
CaO	52.6	52.7	*1.2*	53.2	*2.5*		51.0		51.3	*0.3*	51.7	*1.3*
FeO	1.38	1.60	*0.6*	2.26	*1.5*		1.49		2.50	*0.4*	1.94	*0.8*
MnO	0.05	<0.03	*0.03*	0.04	*0.03*		<0.03		0.04	*0.04*	<0.02	*0.02*
P_2O_5	41.7	39.8	*0.9*	39.5	*2.3*		40.4		39.7	*1.5*	39.2	*0.9*
Na_2O	<0.01	0.50	*0.08*	0.23	*0.34*		0.68		0.54	*0.10*	0.40	*0.08*
K_2O	<0.02	<0.02	*0.02*	<0.01	*0.02*		n.d.		n.d.	—	<0.01	*0.01*
F	5.23	1.17	*0.3*	2.41	*0.4*		2.39		1.48	*0.1*	1.07	*0.4*
Cl	0.41	3.60	*0.5*	0.70	*0.13*		2.21		3.53	*0.4*	4.19	*1.0*
Total	102.15	99.92	*1.2*	100.06	*1.6*		99.14		100.63	*1.3*	99.44	*1.0*
Merrilite												
	Mean (3)	1 analysis		1 analysis		1 analysis	Mean (5)	SD				
SiO_2	0.16	0.85		0.16		0.87	0.54	*0.37*				
Al_2O_3	0.24	0.55		<0.01		0.16	0.06	*0.07*				
MgO	2.93	3.97		3.22		3.60	3.51	*0.4*				
CaO	44.8	43.3		45.8		42.1	45.0	*1.1*				
FeO	1.74	2.42		2.01		4.33	2.03	*0.7*				
MnO	<0.02	<0.01		n.d.		0.05	<0.03	*0.03*				
P_2O_5	45.3	41.7		46.6		42.7	44.3	*1.1*				
Na_2O	2.55	3.21		2.28		2.59	2.77	*0.2*				
K_2O	<0.03	n.d.		0.04		n.d.	<0.03	*0.01*				
F	0.64	0.69		n.d.		0.59	0.73	*0.07*				
Cl	<0.01	0.38		n.d.		0.05	<0.03	*0.02*				
Total	98.36	(97.06)		100.14		(97.06)	98.99	*1.2*				

The number of analyses is given in parentheses. SD = standard deviation; n.d. = not detected.

Table A3. Electron microprobe analyses (wt.%) of troilite and metal within the graphite-containing xenoliths from Krymka.

	Gr1		Gr2		Gr3		Gr4		Gr5		Gr6		Gr7	
Troilite	Mean (28)	SD	Mean (14)	SD	Mean (15)	SD	Mean (15)	SD	Mean (7)	SD	Mean (15)	SD	Mean (14)	SD
Cr	0.04	*0.02*	0.04	*0.02*	0.05	*0.06*	0.07	*0.04*	0.04	*0.02*	0.05	*0.03*	0.04	*0.03*
Fe	62.8	*0.8*	63.2	*0.6*	62.5	*0.6*	63.1	*0.5*	63.3	*0.5*	63.1	*0.3*	63.4	*0.7*
Ni	0.07	*0.09*	0.07	*0.04*	0.16	*0.18*	0.06	*0.05*	0.07	*0.05*	0.06	*0.07*	0.18	*0.09*
Si	0.04	*0.04*	0.06	*0.08*	0.06	*0.03*	0.12	*0.06*	0.04	*0.03*	0.07	*0.06*	0.06	*0.03*
Cu	<0.01	*0.01*	<0.03	*0.04*	0.06	*0.08*	<0.02	*0.03*	<0.01	*0.02*	<0.01	*0.02*	<0.02	*0.03*
Co	<0.03	*0.04*	<0.03	*0.04*	0.06	*0.06*	0.07	*0.05*	0.04	*0.04*	0.06	*0.05*	0.10	*0.06*
S	36.7	*1.4*	35.7	*0.6*	36.1	*0.7*	36.1	*0.7*	35.3	*0.6*	35.2	*0.6*	36.1	*0.7*
P	n.d.	—	<0.01	*0.02*	<0.02	*0.02*	<0.01	*0.02*	<0.01	*0.02*	<0.01	*0.01*	<0.01	*0.01*
Total	99.63	*1.2*	99.05	*0.9*	99.05	*0.7*	99.49	*0.8*	98.83	*0.7*	98.60	*0.5*	99.91	*1.2*
Awaruite														
	Mean (19)	*SD*			Mean (22)	*SD*	Mean (9)	*SD*	Mean (25)	*SD*	Mean (2)		Mean (11)	*SD*
Cr	<0.03	*0.03*			0.04	*0.03*	0.04	*0.04*	0.04	*0.04*	0.04		0.08	*0.05*
Fe	35.8	*2.5*			36.4	*1.8*	38.5	*2.7*	35.6	*1.9*	39.3		41.7	*1.1*
Ni	61.1	*2.6*			60.8	*2.0*	61.0	*2.7*	61.2	*1.9*	58.8		57.3	*1.1*
Si	<0.02	*0.01*			0.10	*0.04*	0.09	*0.02*	0.06	*0.03*	0.09		0.11	*0.03*
Cu	0.07	*0.06*			0.04	*0.06*	<0.02	*0.04*	<0.03	*0.05*	0.11		0.10	*0.06*
Co	2.39	*0.3*			2.44	*0.3*	1.77	*0.3*	2.63	*0.4*	1.73		1.75	*0.4*
S	0.07	*0.08*			0.04	*0.04*	<0.02	*0.02*	0.08	*0.12*	<0.01		<0.03	*0.02*
P	n.d.	—			<0.01	*0.01*	<0.01	*0.01*	<0.01	*0.01*	n.d.		<0.01	*0.02*
Total	99.44	*0.7*			99.87	*1.1*	101.53	*0.4*	99.67	*1.0*	100.00		101.06	*0.8*
Taenite														
	Mean (24)	*SD*			1 analysis		Mean (13)	*SD*	1 analysis		Mean (5)	*SD*	Mean (18)	*SD*
Cr	0.14	*0.03*			<0.03		0.06	*0.05*	0.05		0.15	*0.21*	0.06	*0.05*
Fe	49.2	*1.3*			59.0		49.1	*1.6*	45.4		47.8	*2.1*	60.1	*9.0*
Ni	50.0	*2.0*			42.2		49.8	*1.6*	50.7		51.2	*2.2*	38.1	*8.5*
Si	0.08	*0.06*			0.09		0.18	*0.11*	<0.03		0.10	*0.03*	0.10	*0.12*
Cu	0.14	*0.05*			0.13		0.14	*0.05*	<0.03		0.11	*0.08*	0.09	*0.05*
Co	0.45	*0.04*			0.45		0.48	*0.26*	5.08		0.64	*0.53*	1.51	*0.3*
S	<0.03	*0.05*			<0.03		0.04	*0.03*	0.12		0.05	*0.02*	<0.03	*0.02*
P	0.04	*0.23*			n.d.		<0.03	*0.01*	0.07		<0.02	*0.01*	<0.01	*0.02*
Total	100.07	*0.9*			101.85		99.78	*1.0*	101.46		100.05	*1.2*	100.02	*1.2*
Kamacite														
			1 analysis				Mean (7)	*SD*			1 analysis		1 analysis	
Cr			0.04				0.10	*0.03*			0.15		0.59	
Fe			95.9				93.3	*1.1*			89.9		91.0	
Ni			4.27				4.29	*0.7*			4.07		4.47	
Si			0.10				0.09	*0.05*			0.15		0.10	
Cu			0.10				<0.03	*0.03*			n.d.		n.d.	
Co			2.21				1.99	*0.2*			2.87		0.38	
S			<0.03				<0.03	*0.03*			<0.03		0.09	
P			n.d.				<0.01	*0.03*			0.07		n.d.	
Total			(102.66)				99.83	*1.3*			(97.21)		(96.65)	

The number of analyses is given in parentheses. SD = standard deviation; n.d. = not detected.

Table A4. Electron microprobe analyses (wt.%) of chromites within the graphite-containing xenoliths from Krymka.

	Gr1			Gr2	Gr3			Gr4		Gr5		Gr6		Gr7		
	Mean (11)	SD	Mean (3)	Mean (2)	Mean (10)	SD	1 analysis	Mean (6)	SD	Mean (3)	SD	Mean (5)	SD	Mean (12)	SD	Mean (2)
SiO_2	0.22	*0.59*	0.27	0.28	0.53	*1.00*	0.24	0.53	*0.30*	0.18	*0.02*	0.33	*0.12*	0.17	*0.23*	0.24
Al_2O_3	11.4	*0.6*	3.79	14.5	10.5	*0.3*	6.89	14.5	*0.5*	11.9	*0.1*	7.50	*0.1*	3.95	*0.1*	6.21
MgO	3.14	*0.3*	1.82	2.19	3.17	*0.3*	2.21	2.09	*0.1*	3.38	*0.0*	1.38	*0.1*	1.87	*0.1*	6.64
TiO_2	4.00	*0.2*	1.50	2.93	3.24	*0.5*	2.09	2.89	*0.5*	3.63	*0.0*	4.40	*0.1*	2.86	*0.2*	0.87
CaO	0.08	*0.07*	0.17	0.16	0.39	*0.58*	0.08	0.07	*0.03*	0.07	*0.02*	0.05	*0.02*	0.10	*0.05*	0.12
FeO	32.8	*0.8*	31.6	34.0	33.0	*0.8*	36.5	34.3	*2.2*	32.5	*0.2*	33.3	*0.5*	32.3	*0.9*	23.9
MnO	0.30	*0.04*	0.44	0.32	0.39	*0.09*	0.44	0.33	*0.09*	0.37	*0.06*	0.40	*0.02*	0.52	*0.07*	0.50
Cr_2O_3	46.4	*0.8*	58.3	43.1	47.0	*1.3*	49.0	43.1	*1.4*	45.9	*0.1*	50.7	*0.9*	57.4	*0.9*	62.1
V_2O_3	0.48	*0.10*	0.71	0.47	0.61	*0.11*	0.67	0.42	*0.09*	0.54	*0.00*	0.62	*0.02*	0.68	*0.05*	0.73
Total	98.78	*0.6*	98.57	98.04	98.79	*1.01*	98.13	98.31	*0.9*	98.47	*0.4*	98.71	*0.7*	99.84	*1.3*	101.34
FeO[a]	31.1	*1.6*	28.8	32.3	30.3	*1.8*	30.4	32.5	*0.3*	30.9	*0.1*	33.2	*0.4*	31.5	*0.7*	23.2
Fe_2O_3[a]	1.73	*1.3*	3.09	1.88	3.00	*1.3*	6.79	1.98	*2.7*	1.75	*0.1*	0.07	*0.15*	0.91	*0.58*	0.86

The number of analyses is given in parentheses. SD = standard deviation.
[a] Recalculated contents.